MATHEMATICAL MODELING AND NUMERICAL SIMULATION OF POLYMER ELECTROLYTE MEMBRANE FUEL CELLS

By

Eng. Ammar Mohamed Abd-Elghany Mohamed

A Thesis Submitted to the Faculty
of Engineering at Cairo University
in Partial Fulfillment of the
Requirements for the Degree of
MASTER OF SCIENCE

In

MECHANICAL POWER ENGINEERING

FACULTY OF ENGINEERING, CAIRO UNIVERSITY
GIZA, EGYPT
2004

MATHEMATICAL MODELING AND NUMERICAL SIMULATION OF POLYMER ELECTROLYTE MEMBRANE FUEL CELLS

By

Eng. Ammar Mohamed Abd-Elghany Mohamed

A Thesis Submitted to the Faculty of
Engineering at Cairo University
in Partial Fulfillment of the
Requirements for the Degree of
MASTER OF SCIENCE

In

MECHANICAL POWER ENGINEERING

Under Supervision of

Prof. Dr. Hany A. S. E. Khater
Mechanical Power Department
Faculty of Engineering
Cairo University

Prof. Dr. Hindawy S. Mohamed
Mechanical Power Department
Faculty of Engineering
Cairo University

Dr. Amr M. A. Abdel-Raouf
Mechanical Power Department
Faculty of Engineering
Cairo University

FACULTY OF ENGINEERING, CAIRO UNIVERSITY
GIZA, EGYPT
2004

MATHEMATICAL MODELING AND NUMERICAL SIMULATION OF POLYMER ELECTROLYTE MEMBRANE FUEL CELLS

By

Eng. Ammar Mohamed Abd-Elghany Mohamed

A Thesis Submitted to the Faculty
of Engineering at Cairo University
in Partial Fulfillment of the
Requirements for the Degree of
MASTER OF SCIENCE

In

MECHANICAL POWER ENGINEERING

Approved by the
Examining Committee

Prof. Dr. Samir M. Abd-Elghany	**Member**
Prof. Dr. Mohsen M.M. Abu-Ellail	**Member**
Prof. Dr. Hany A.S.E. Khater	**Main Advisor**
Prof. Dr. Hindawy S. Mohamed	**Advisor**

FACULTY OF ENGINEERING, CAIRO UNIVERSITY
GIZA, EGYPT
2004

CONTENTS

LIST OF TABLES

LIST OF FIGURES

LIST OF SYMBOLS AND ABBREVIATIONS

Symbol	QUANTITY	Units
V	Cell voltage	Volt
F	Faraday's constant	C/mol
T	Temperature	K
Y	Species mass fraction	
u	Velocity vector	m/s
P	Pressure	Pa
R	Universal gas constant	kJ/kmol.K
i	Current density	A/m^2
A	Electrode area	m^2
ν_+^o	Volumetric flow rate	m^3/s
D_k	Mass Diffusivity of species k	m^2/s
X	Species mole fraction	
C	Species concentration	mol/m^3
z_f	Fixed site charge	
K	Permeability	m^2
$Eff_{\max}$	Carnot cycle efficiency	
S	Entropy	kJ/K
H	Enthalpy	kJ
i	Current density	A/m^2
I	Current	A
n	Number of electrons per kmol of fuel	
R	Gas constant	kj/kmol.K
r	Component resistance	Ω
A	Electrode area	m^2
$\dot{n}$	Molar flow rate	mol/s
aj	Exchange current density×Electrode area	A/m^3
M	Molecular mass	kg/kmol
L	Gas channel length	m

Greek Letters

Symbol	QUANTITY	Units
η	Overpotential	Volt
μ	Dynamic viscosity	Pa.s
ρ	Density	kg/m^3
σ	Protonic conductivity	S/m
α	Charge Transfer coefficient	
Φ	Membrane phase potential	Volt
ζ	Stoichiometric flow ratios	
ϵ	Porosity	

Chemical Symbols

CO	Carbon Monoxide
H_2	Hydrogen
H_2O	Water
O_2	Oxygen
N_2	Nitrogen

Subscripts

a	Activation
avg	Average
m/c	Mass/concentration
r	Ohmic
ex	Exit value
in	Inlet value
+	Value at the cathode side
-	Value at the anode side
oc	Open-circuit value
l	Limiting value
ref	Value at reference/standard conditions
Dc	Darcy
H_2	Value for hydrogen
O_2	Value for oxygen
H_2O	Value for water
sat	Saturation

Superscripts

*	Guessed value for a field parameter
-	Corrected value for a field parameter
o	Value at equilibrium or reference conditions

Abbreviations

AFC	Alkali fuel cell
AC	Alternating current
CFD	Computational Fluid Dynamics
CL	Catalyst layer
DC	Direct current
DMFC	Direct Methanol Fuel Cell
GDL	Gas diffusion layer
LHV	Lower Heating Value
MCFC	Molten Carbonate Fuel Cell
ORR	Oxygen Reduction Reaction
PAFC	Phosphoric Acid Fuel Cell
PEMFC	Proton Exchange Membrane Fuel Cell / Polymer Electrolyte Membrane Fuel Cell
PLDS	Power Law Difference Scheme
QUICK	Quadratic Interpolation Scheme
SOFC	Solid Oxide Fuel Cell
VTC	Voltage-to-Current

To My Constant Companion, Confidant
And Shoulder; ***My Father***.
May Allah Rest his Soul. Amen.

ACKNOWLEDGEMENT

I would like to express my deep gratitude to my Advisors who provided support, vision and insight in every step of the way to accomplish this thesis work. My heartfelt thanks are due to Prof. **Hany A.S.E. Khater** for superbly managing and orchestrating an enormous amount of detail and ideas in this thesis work and for reviewing the first drafts with a critical eye to make suggestions for improvements.

Many thanks go to Prof. **Hindawy S. Mohamed** for his help and support during the various stages of this thesis work. His insightful comments and notes both favorable and critical were of great significance for this work.

I am grateful to Dr. **Amr M.A. Abdel-Raouf** for his great help and support during the time of this work. His contributions were of great impact on this work.

Special thanks go to Prof. B.E. Launder and Prof. M.A. Leschziner at the UMIST for mailing me the TEAM CFD code manual.

I also wish to thank my colleagues, professors at the Mechanical Power Department especially Prof.Mohsen Abu-Ellail, Prof. Abd-Elmotalib Mostafa, and all those I love for their strong shoulders, no matter what their size.

Finally, I would like to acknowledge the excellent help, atmosphere, patience, tolerance and cooperation that my family provided me during the painstaking period of my MSC thesis. A very special thank you to my father- may Allah rest his soul- for his encouragement, advice and admonishment throughout the period of both my BSC and MSC, until the day he passed away. Had it not been for all he gave me, this work would have not been possible.

ABSTRACT

Fuel Cells are one of the most promising power generation techniques due to their high efficiency with much lower thermal and acoustic harmful emissions that result from fuel-air reactions. These cells are also advantageous for their mobility and size flexibility that enable usage in different applications. They are so able to spread over different sites where clean electric power is needed and are thus a reliable alternative to conventional internal combustion engines and steam power plants as well.

In this thesis, a single phase, steady-state, two-dimensional model has been developed to simulate proton exchange membrane fuel cells. The model accounts simultaneously for electrochemical kinetics, hydrodynamics, and multicomponent transport. A single set of conservation equations valid for the heterogeneous domain consisting of the flow channels, gas-diffusion electrodes, catalyst layers, and the membrane region was developed and numerically solved using an in-house CFD code utilizing the efficient PISO algorithm. The numerical solution shed light on the complex electrochemistry-flow/transport interactions in the fuel cell and was used to investigate the effect of the different cell operating conditions like temperature, pressure and reformate composition (viz. inlet hydrogen percent) on the performance of the fuel cell. The numerical model was validated against published experimental data as well as other numerical solutions and was found to be in good agreement. The detailed two-dimensional electrochemical and flow/transport simulations further revealed that in the presence of pure oxygen in the cathode stream mass transport limitations (which limit the cell performance) are alleviated leading to increased cell current density and better performance. In a like manner but to some lesser extent, the presence of hydrogen dilution in the anode resulted in anode mass transport polarization and hence a lower current density that is limited by hydrogen transport from the anode stream to the active reaction sites. Eventually, the current density identifying the onset of two-phase flow regime (which limits the applicability of the present model) is predicted.

Chapter One
INTRODUCTION

As environmental concerns receive increasing attention, the need for developing new technologies that address the conflicting issues of energy production and protection of the environment becomes evident. The extraordinary environmental quality and high efficiency of fuel cells make them a potential alternative energy source for both stationary and transportation applications. Fuel cells have the opportunity to end the carbon-dominated energy system of the 20th century and make the most of the broadly available hydrogen molecule [1]. While fuel cell technology matures and further research advances are made, the challenge for the fuel cell industry will be to commercialize fuel cell systems by improving their performance and cost. This chapter gives a general introduction to fuel cells with an emphasis on polymer electrolyte membrane fuel cells (PEMFCs) and presents the objectives for this thesis work.

1.1 Fuel Cells

1.1.1 Overview of Fuel Cells

A fuel cell is an electrochemical device that converts the chemical energy of a reaction directly into electrical energy. Since it operates without combustion, it is virtually pollution free [1]. Typically, a fuel cell consists of two porous electrodes (viz.anode and cathode) separated by an electrolyte layer allowing ions transfer between the electrodes to complete the electric circuit. Gaseous fuels (hydrogen) are fed to the anode and the oxidant (in general, the oxygen in the air) is fed at the cathode by the way of flow channels cut into two electronically conductive collector plates. At the anode, the fuel catalytically splits into ions and electrons. The electrons go through an external circuit to provide electric current while the ions move through the electrolyte towards the opposite electrode (see figure 1.1). Depending on the nature of the electrolyte, different reactions will occur at the electrodes. As a result of

[1] In fact, if a fuel cell, as opposed to fuel cell systems, operates on neat H_2 then it is pollution free. If, However, it operates on reformate (a mixture of H_2 and other gases such as CO and CO_2) then some Pollution will occur but at levels significantly below that of conventional combustion devices [1].

This process, heat is generated and water is produced. Since an individual fuel cell produces approximately one Volt at full load, fuel cells are stacked in series to produce usable voltages.

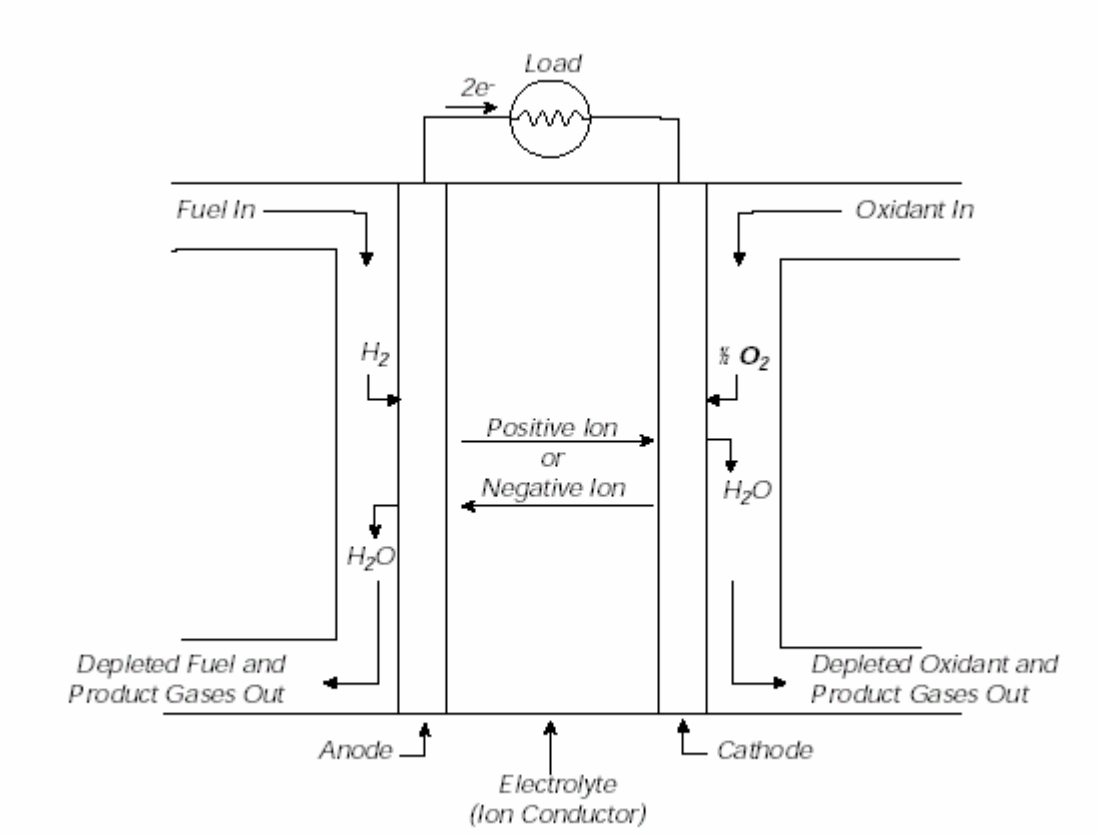

Figure 1.1 Individual fuel cell schematic [1]

The hydrogen necessary for fuel cell operation is not naturally occurring as a gaseous fuel and must, therefore, be generated from another primary fuel via a fuel processor (external reforming) before being fed into the fuel cell or the fuel cell stack. Some fuel cell operating temperatures are high enough that the reforming reaction can actually occur within the cell (internal reforming). In addition, the electric power generated by the stack needs to be converted from DC to AC for many applications. Water generated and that used for humidification requires management, and heat generated must be removed in order to maintain a constant fuel cell operating temperature. As a result, a complete fuel cell system includes a fuel processor, the fuel cell stack, a power conditioner, and both heat and water management sub-systems (see Figure 1.2).

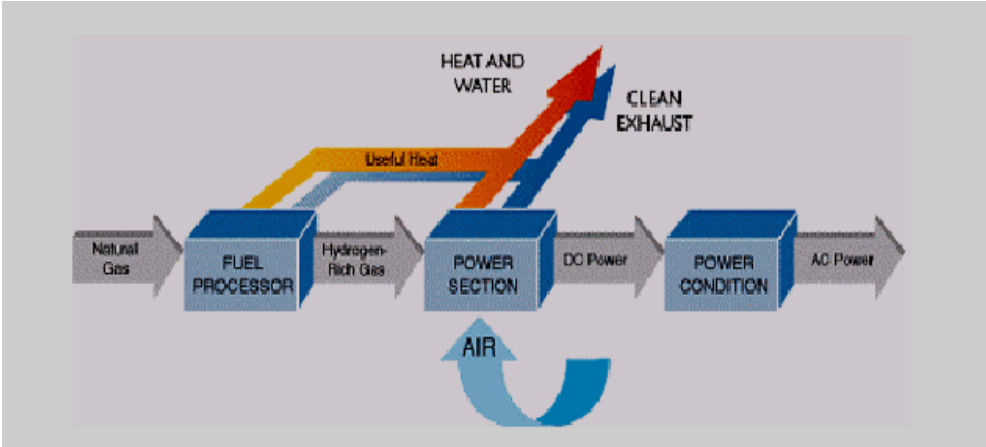

Figure 1.2 A fuel cell system with external reforming (US Department of Defense).

1.1.2 Characteristics

As mentioned earlier, fuel cells have many characteristics that make them a possible Alternative to conventional energy conversion systems:

- *Efficiency:* because they convert chemical energy directly into electrical energy, fuel cell efficiencies are not limited to the Carnot limit. Therefore, even at low temperature, they are potentially more efficient than internal combustion engines. Efficiencies of present fuel cell plants are in the range of 40 to 55 % [2], and hybrid fuel cell/gas reheat turbine cycles have demonstrated efficiencies greater than 70 % [1]. In addition, the efficiency is nearly independent of the electric load down to a small fraction of full load. This makes fuel cells very suitable for applications such as vehicles, where good efficiency is desired even far from peak power (full load).
- *Low emissions:* when pure hydrogen is used directly as a fuel, only water is created and no pollutant is rejected. However, the processing of hydrocarbon fuels into hydrogen can result in a small output of NO_x, SO_x, CO, and an amount of CO_2 significantly lower when compared, for example, to classical internal combustion engines.

[2] Based on the lower heating value (LHV) of the fuel [1].

- *Cogeneration capability:* the exothermic chemical and electrochemical reactions produce usable heat. That could be used in cogeneration applications that are frequently referred to as combined heat and power CHP applications.
- *Scalability:* fuel cells can be configured to suit a wide range of sizes for applications, ranging from a few watts to megawatts. Thus, fuel cells are expected to serve as a power source for portable computers as well as vehicles or large power plants.
- *Fuel flexibility:* fuel cells can be operated using commonly available fuels such as natural gas, methanol, and various complex hydrocarbons.
- *Reliability and low maintenance:* the absence of moving parts reduces the maintenance requirements and minimizes system down-time.
- *Quiet operation.*

In spite of these many positive characteristics, additional improvements in fuel cell technology are needed with the focus of the reduction of the high cost of current fuel cell systems as well as the development of the infrastructure necessary for the widespread use of hydrogen fuel.

1.1.3 Different Types of Fuel Cells

Fuel cells are usually classified by the nature of the electrolyte they use. Table 1.1 summarizes the major technical differences between them. These distinctions allow one to choose the type of fuel cell that best matches a given application. As shown in Table 1.1, PEMFCs deliver significantly higher power density than the other types of fuel cells, with the exception of the AFC and SOFC, which have comparable performance. Their electrical efficiency of 40 to 55 % is also relatively high in comparison to the efficiency of a spark-ignition internal combustion (IC) engine of comparable size (e.g., 37.6 % at full load [2]). For compression-ignition IC engines, this efficiency at full load compares favorably (e.g. 48 % at full load [2]). It is however; at partial load that the fuel cell system has a significant advantage over both of these types of IC engines.

Table 1.1 Characteristics of different types of fuel cells.

Fuel Cell Type	Proton Exchange Membrane (PEMFC)	Alkaline (AFC)	Phosphoric Acid (PAFC)	Molten Carbonate (MCFC)	Solid Oxide (SOFC)
Mobile Ion	H^+	OH^-	H^+	CO_3^{2-}	O^{2-}
Operating Temperature (°C)	50 - 100	50 – 200	~ 220	~ 650	600 - 1000
Power Density (kW/m^2)	3.8 – 2.6	0.7 – 8.1	0.8 – 1.9	0.1 – 1.5	1.5 – 2.6
Reforming	external	external	external	external or internal	external or internal
Electrical 1st Law Efficiency (%)	40 – 55 (stack)	45 – 60 (stack)	40 – 50 (stack) 41 (system)	50 – 60 (system)	50 – 65 (stack) 45 – 50 (system)
Start-up Time	sec – min	min	hours	hours	hours

.

In addition, the low operating temperature of the PEMFC allows for quick startup and fast response to changes in electrical load. These characteristics, along with their relatively long expected lifetime, make the PEMFC a very suitable power system for vehicular applications as well as small stationary power plants. .

1.1.4 Fuel Cell Efficiency

Because a fuel cell directly converts chemical energy into electrical energy, the maximum theoretical efficiency is not bound by the Carnot cycle, and can be shown as in [3]:

$$Eff_{\max} = 1 - T\,\Delta S/\Delta H \qquad (1.1)$$

Values calculated from Eq. (1.1) range from 60-90%. As an example, a hydrogen fuel cell with water vapor as product has a maximum possible operating efficiency of 80% at an operating temperature of 100 °C, and 60% at 1000 °C. In practice, however, higher temperature operation results in reduced activation polarization, and the

difference in actual operating efficiency with temperature is less significant. In practice, a 100 kW system operated by Dutch and Danish utilities has already demonstrated an operating efficiency of 46% (LHV) over more than 3700 hours of operation, according to [4]. Combined fuel cell/bottoming cycle and cogeneration plants promise operational efficiencies as high as 80%, with very low pollution. Another major advantage of fuel cells compared to heat engines is that efficiency is not a major function of device size, so that high efficiency power for portable electronics can be realized, whereas small scale heat engines can only reach system efficiencies of 10-15%. While advanced automotive direct injection heat engine efficiencies can achieve 28%, with little hope of significant future gains, future fuel cell systems can achieve nearly 40% [5].

1.1.5 Basic Fuel Cell Operation

Figure 1.3 shows a generalized schematic of a fuel cell. The drawing is not to scale because it represents a generalized fuel cell system. Electrochemical reactions for the anode and cathode are shown for a hydrogen-fed polymer electrolyte membrane fuel cell (H_2 PEMFC), a direct methanol fuel cell (DMFC), and a solid oxide fuel cell (SOFC). Liquid or gas-phase fuel and oxidizer streams enter through flow channels, separated by the electrolyte/electrode assembly. Reactants are transported by diffusion and/or convection to the catalyzed electrode surfaces, where electrochemical reactions take place. In PEM fuel cells (these include H_2 and DMFC), transport to the electrode takes place through an electrically conductive carbon paper or carbon cloth backing layer, which covers the electrolyte on both sides. These backing layers (have a typical porosity value of 0.3-0.8) serve the dual purpose of transporting reactants and products to and from the electrode and electrons to and from the bipolar plates to the reaction site [5]. An electrochemical oxidation reaction at the anode produces electrons that flow through the bipolar plate/cell interconnect to the external circuit, while the ions pass through the electrolyte to the opposing electrode. The electrons return from the external circuit to participate in the electrochemical reduction reaction at the cathode.

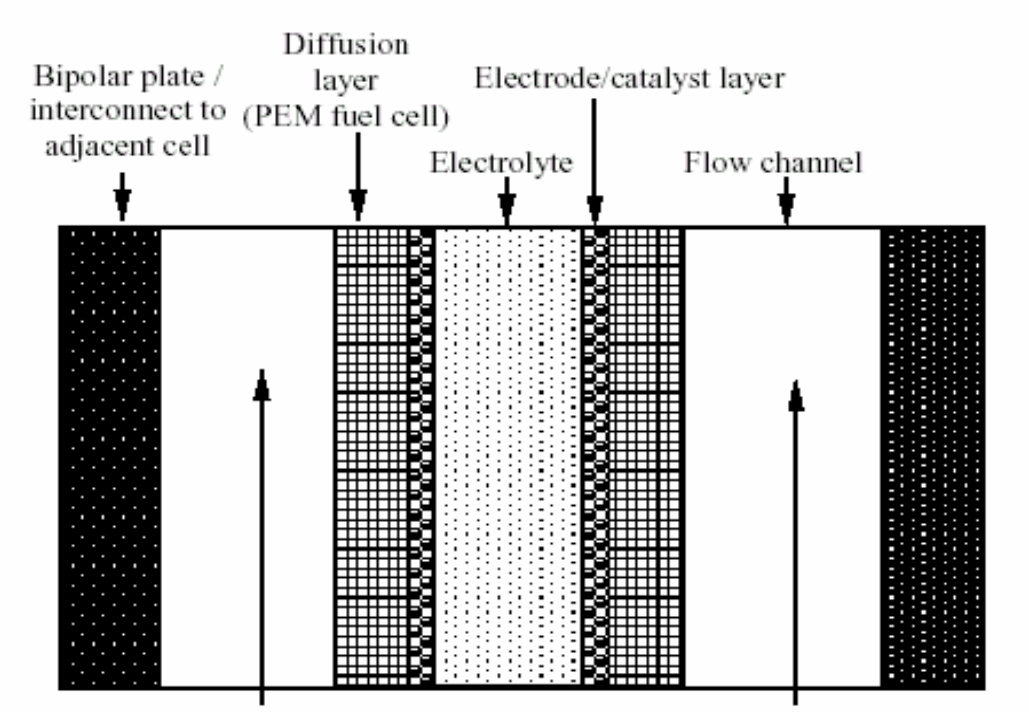

Anode Reaction:

$\underline{H_2\ \text{PEM}}$: $H_2 \rightarrow 2H^+ + 2c$

$\underline{\text{DMFC}}$: $CH_3OH + H_2O \rightarrow CO_2 + 6H^+ + 6e^-$

$\underline{\text{SOFC}}$: $H_2 + O^{-2} \rightarrow H_2O + 2e^-$

$CO + O^{-2} \rightarrow CO_2 + 2e^-$

Cathode Reaction:

$\underline{H_2\ \text{PEM}}$: : $O_2 + 4e^- + 4H^+ \rightarrow 2H_2O$

$\underline{\text{DMFC}}$: $6H^+ + 6e^- + 3/2O_2 \rightarrow 6H_2O$

$\underline{\text{SOFC}}$: $1/2O_2 + 2e^- \rightarrow 2O^{-2}$

FIGURE 1.3 Generalized schematic of a single fuel cell [5].

1.1.6 Performance Characterization

The single cell combination shown in Figure 1.3 provides a voltage dependent on operating conditions such as temperature, applied load and fuel/oxidant flow rates. Figure 1.4 is an illustration of a polarization curve for a fuel cell. The polarization curve, which represents the cell voltage behavior against operating current density, is the standard measure of performance for fuel cell systems. There are three major classifications of losses that result in a drop from the open circuit voltage: 1) activation polarization, 2) ohmic polarization, and 3) concentration polarization. The

operating voltage of a fuel cell can be represented as the departure from ideal voltage caused by these polarizations:

$$V_{cell} = V_{oc} - \eta_{a,a} - \eta_{a,c} - \eta_{r} - \eta_{m,a} - \eta_{m,c} \qquad (1.2)$$

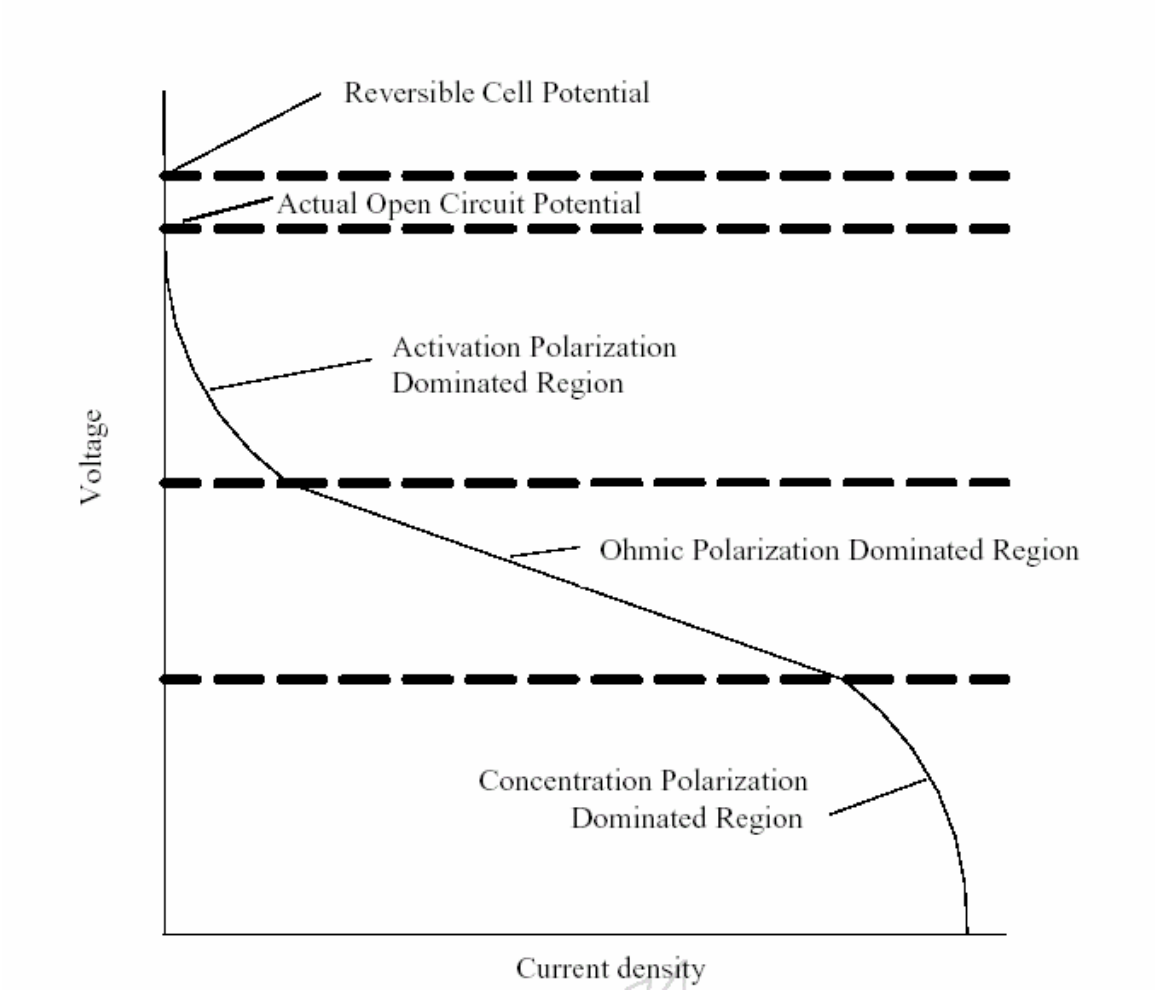

FIGURE 1.4 Generalized polarization curve for a fuel cell showing regions dominated by various types of losses [5].

Where V_{oc} is the open circuit potential of the cell, and η_a, η_r, and η_m represent activation, ohmic (resistive) and mass concentration polarization. Activation and concentration polarization occurs at both anode and cathode locations, while the resistive polarization represents ohmic losses throughout the fuel cell. Activation polarization, which dominates losses at low current density, is the voltage overpotential required to overcome the activation energy of the electrochemical reaction on the catalytic surface, and is thus similar to the activation energy of purely

chemical reactions. Activation polarization is a measure of the catalyst effectiveness at a given temperature, and is thus primarily a material science and electrode manufacturing issue. This type of overpotential can be represented by the Tafel equation at each electrode, as described by [6]:

$$\eta_{a,a} + \eta_{a,c} = \frac{\overline{R}T}{nF\alpha}\ln\left(\frac{i}{i_o}\right)\Bigg|_a + \frac{\overline{R}T}{nF\alpha}\ln\left(\frac{i}{i_o}\right)\Bigg|_c \qquad (1.3)$$

Where α is the charge transfer coefficient and can be different between anode and cathode, and represents portion of the electrical energy applied that is used to change the rate of electrochemical reaction. In this case, n is the number of exchange electrons per mole of reactant, and F is Faraday's constant. The exchange current density, i_o, represents the activity of the electrode for a particular reaction at equilibrium. In hydrogen PEM fuel cells, the anode i_o for hydrogen oxidation is so high, relative to the cathode i_o for oxygen reduction, that the anode contribution to this polarization is often neglected. On the contrary, direct methanol fuel cells suffer significant activation polarization losses at both electrodes. For SOFCs, the operating temperatures are so high that there are very low activation polarization losses. It appears from Eq. (1.3) that activation polarization should increase linearly with temperature. However, i_o is a function of the kinetic rate constant of reaction which is commonly modeled with an Arrhenius form, and thus i_o is an exponentially increasing function of temperature [6]. Therefore, the net effect of increasing temperature is to decrease activation polarization. Accordingly, an effect of an increase in temperature would be to decrease the voltage drop within the activation polarization region shown in Fig. 1.4. At increased current densities, a primarily linear region is evident on the polarization curve. In this region, reduction in voltage is dominated by internal ohmic losses (η_r) through the fuel cell that can be represented as:

$$\eta_r = I(\sum r_k) \qquad (1.4)$$

Where each r_k value is the resistance of individual cell components, including the ionic resistance of the electrolyte, and the electric resistance of bipolar plates, cell interconnects, contact resistance between mating parts and any other cell components through which electrons flow. With proper cell design, ohmic polarization is typically

dominated by electrolyte conductivity. Electrolyte conductivity is primarily a function of water content and temperature in PEM fuel cells, and operating temperature in SOFCs, thus water transport is an especially important issue in PEM fuel cell design even a slight reduction in ohmic losses through advanced materials, thinner electrolytes, or optimal temperature/water distribution can significantly improve fuel cell performance and power density[5]. At very high current densities, mass transport limitation of fuel or oxidizer to the corresponding electrode causes a sharp decline in the output voltage. This is referred to as concentration polarization. This region of the polarization curve is solely a mass transport related phenomenon, and creative means of facilitating species transport to the electrode surface can result in greatly improved performance at high current density and fuel utilization conditions. The Damkler number (Da) is a dimensionless parameter that is the ratio of the characteristic electrochemical reaction rate to the rate of mass transport to the reaction surface. In the limiting case of infinite kinetics (high Damkler number), one can derive an expression for η_m based on the Tafel expression as:

$$\eta_m = -\frac{RT}{nF}\ln(1-\frac{i}{i_l}) \qquad (1.5)$$

Where i_l is the limiting current density, and represents the maximum current produced when the surface concentration of reactant is reduced to zero at the reaction site. In reality, however, the assumption of a completely mass-transfer limiting case is rarely valid because there is a concentration dependence in the activation kinetics of reaction that affects activation polarization as well. In addition, the Tafel expression is not appropriate near equilibrium conditions and another function must be used. Near equilibrium and in cases of mixed kinetic/mass transfer limitation, a Butler-Volmer expression can be applied to express the resulting current density with a concentration dependence of the reactants (see, for example [7]), although no explicit expression for η_m can be written.

The appropriate mass flow rate of reactants is determined by several factors relating to several requirements such as the minimum requirement for electrochemical reaction, maintaining proper water balance and thermal management. In various situations, water management concerns may dictate the need for increased flow rate, for example. However, the minimum flow requirements for all fuel cells are

determined by the requirements of the electrochemical reaction. An expression for the molar flow rate of species required for electrochemical reaction can be shown as:

$$\dot{n}_{\text{reactant}} = \frac{iA}{nF} \qquad (1.6)$$

Where i and A represent the current density and total electrode area, respectively. The stoichiometric ratio for an electrode reaction is defined as the ratio of reactant provided to that needed for the electrochemical reaction of interest.

1.2 Proton Exchange Membrane Fuel Cells

1.2.1 Design and Operation

A PEMFC uses a polymer electrolyte membrane usually made of Nafion® (from DuPont), whose chemical structure consists of a fluorocarbon polymer with sulfonic acid groups attached. Through this structure, the protons and water molecules are free to migrate. However, the Nafion® material remains impermeable to reactants (hydrogen at the anode and oxygen at the cathode) and is a good electronic insulator. The membrane is sandwiched between the two electrodes on which a small amount of platinum catalyst has been deposited at the membrane interfaces to form the catalyst layers. The catalyst particles are supported by the electrode material, which can be considered as a thin sheet of porous carbon paper that has been wet-proofed with Teflon®. The carbon fiber material is also referred to as the backing layer. These components produce a membrane electrode assembly or MEA (see figure 1.5). This structure is about 725 microns thick, the electrodes being approximately 300 microns each and the catalyst layers 10 microns each. The MEA is connected on each side to electronically conductive collector plates, which supply the fuel and the oxidant to the electrodes via gas channels and conduct the current to the external circuit. The reactants are transported by diffusion through the porous electrodes to the reaction site. At the anode, the oxidation of hydrogen fuel releases hydrogen protons that are transported through the membrane and electrons that produce the electrical current. At the cathode, oxygen reacts with the protons and electrons to produce liquid water. Figure 1.6 summarizes the main phenomena in a PEMFC.

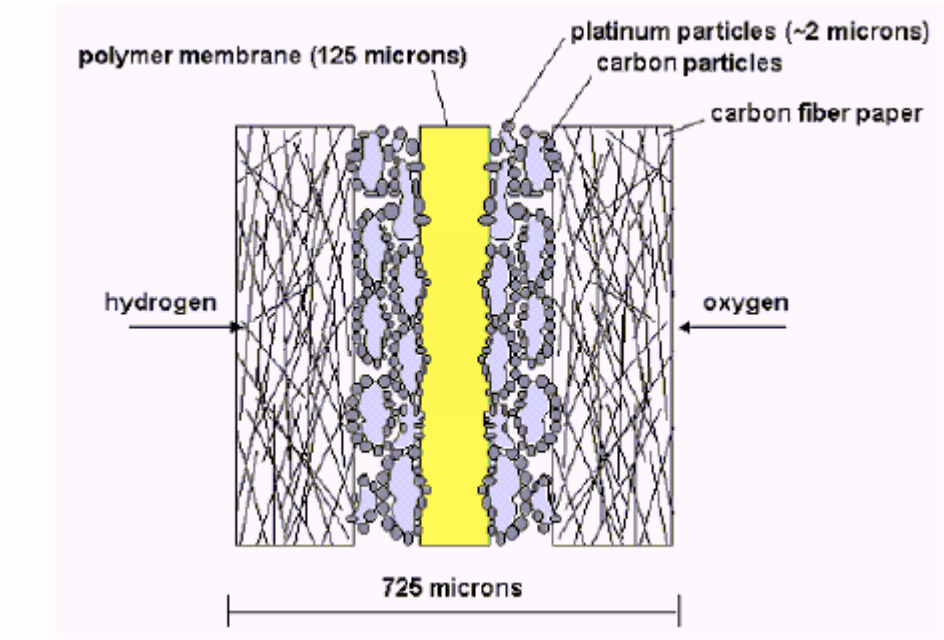

Figure 1.5 a membrane-electrode assembly [8]

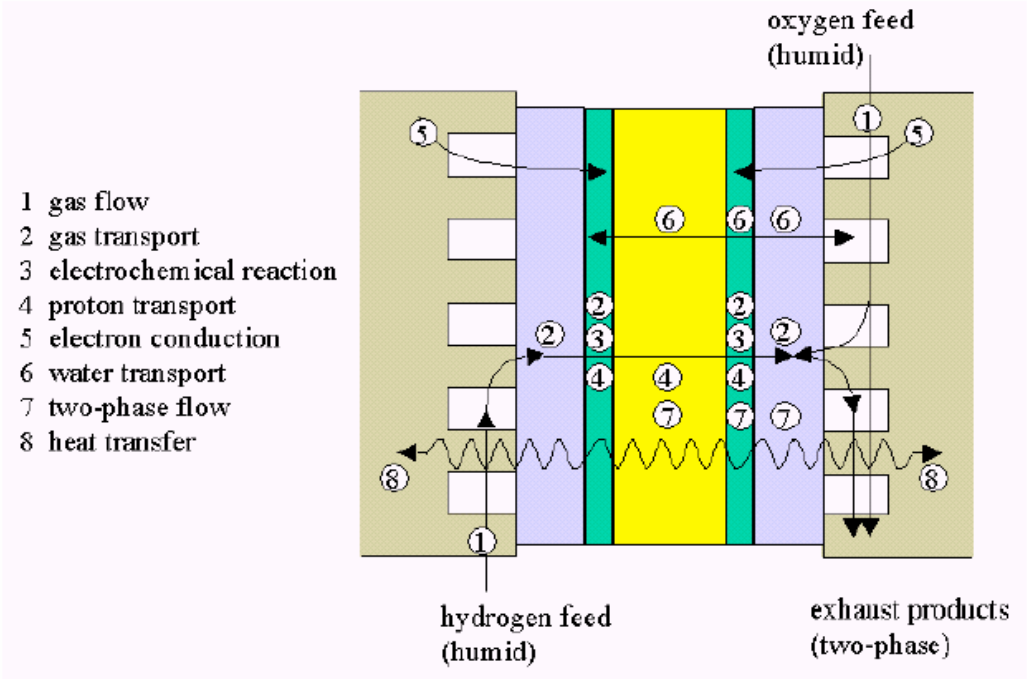

Figure 1.6 Phenomena in a PEMFC [8]

The electrochemical reactions are

$$H_2 \leftrightarrow 2H^+ + 2e^- \qquad \text{(Anode)}$$

$$2H^+ + \frac{1}{2}O_2 + 2e^- \leftrightarrow \mathrm{H_2O} \qquad \text{(Cathode)}$$

The overall reaction is

$$H_2 + \frac{1}{2}O_2 \leftrightarrow \mathrm{H_2O}$$

1.2.2 Performance issues

Fuel cell performance is affected by many parameters. To ensure good cell operation, The following issues need to be addressed:

- *Reactant distribution:* the concentration of each reactant at the interface between the gas channels and the electrodes must be uniformly distributed in order to avoid losses due to concentration polarization.
- *Water management:* in order to ensure good proton conductivity, the polymer membrane must remain hydrated. It is also necessary to avoid damage to the membrane structure. However, too much water could result in flooding in the electrodes, blocking the pores that allow reactant transport, and affecting the reaction rate. Therefore, it is necessary to balance these two phenomena. Sources of water in a fuel cell include the water vapor which is transported by the reactants flow both at the anode and cathode sides, since the reactants are usually humidified to help ensure membrane hydration. In addition, at the cathode, water is produced during the electrochemical reaction, providing another source for membrane hydration. Excess water at the cathode can be removed toward the gas channels thanks to the capillary forces that result from the partial evaporation of liquid water in the pores of the backing layer [9]. Water is, furthermore, transported in the membrane by convection due to a pressure gradient between the electrodes, by diffusion due to a concentration gradient, and by the drag force caused by proton migration. When combined together, the action of these phenomena can result in an uneven water distribution in the membrane. For example, at high current densities, the anode side may dry out even if the cathode side remains hydrated. Fortunately, all of these phenomena of water movement can be predicted and controlled.

- *Transport properties in the catalyst layer and the catalyst effective utilization:* the cost of the catalyst material is critical. In order to ensure the best utilization of the catalyst layer, the reactants need to be transported at a uniform rate to the reaction site at the surface of the agglomerates of Teflon® and platinum particles (see Figure 1.5). Reactant transport occurs within the pores separating these agglomerates, while proton transport occurs in the polymer phase. The transport of reactants becomes a limiting factor if too much resistance is offered to diffusion of species in the pores. This can occur at high current densities, or in the case of flooding due to excess liquid water. In these cases, the catalyst layer is not utilized in its totality [9].
- *Heat management:* temperature can affect the material properties of the cell components and, therefore, cell performance. It is important to remove the heat that is produced within the cell by ohmic heating, phase change and electrochemical reaction and, thus, insure a homogeneous cell temperature. In general, the critical factor that determines maximum cell operating temperature is the membrane material. In a PEMFC, this temperature is about 80 °C

1.3 Thesis Objectives

In this thesis work, much emphasis has been laid on the PEMFC. The main target was to analyze in detail the different aspects of operation of this widely spread type of fuel cells. In order to do this, a fundamental understanding of the physical phenomena occurring within the cell is a must. The objectives for my thesis work could best be summarized as follows:

- To understand the mathematical formulation of the heat, mass phenomena as well as electrochemical phenomena in the PEMFC developed by Um et al.2000 [7].
- To suggest modifications to this model if warranted and implement them.
- To develop a numerical algorithm for solving the proposed mathematical model.

- To understand and modify as necessary the research finite Volume code "TEAM" developed by P.G. Huang, B.E. Launder and M.A. Leschziner at the university of Manchester 1984
- To validate the model using experimental data as well as numerically predicted data found in the literature.
- To generate an extensive set of results and perform a detailed analysis of the phenomena present to more thoroughly understand the physics underlying the operation of the PEMFC.
- To make some recommendations for future work which could lead to improvements of the existing model and possibly lead to more in-depth understanding and addressing of performance issues of the PEMFC.

Chapter Two
Fuel Cells Modeling

2.1 Literature Survey

Most current fuel cell models have been developed to only individually address the PEMFC performance issues. None of them consider the fuel cell stack as a whole so as to deal simultaneously with all the phenomena. In addition, the experimental data and mathematical models found in the literature are valid only under specific assumptions and idealized conditions that are quite often unrealistic. Nevertheless, some of the most pertinent contributions to the mathematical modeling of a PEMFC are presented in this chapter.

In 1991, at the Los Alamos National Laboratory, Springer et al. [10] presented a one-dimensional steady-state isothermal model of a complete fuel cell to mainly investigate the water transport mechanisms within the membrane and to experimentally study the effect of the membrane protonic conductivity on the water transport and on the overall cell performance. The model was designed for water in the vapor state in the cathode but can accommodate some excess liquid water - assumed to be finely dispersed- and it yielded some successful predictions, in agreement with the experiment but only for conditions where excess water was not present. One of the discrepancies they found out is that their model does not predict the need to humidify the cathode feed stream continuously at any appreciable current density while they experimentally found that the highest performance is achieved with well-humidified cathode feed streams.

In 1992 Bernardi et al. [11] developed a one-dimensional steady-state isothermal model of a PEMFC that makes use of the Pseudo-homogeneous catalyst layers modeling approach. They studied the factors that limit the cell performance and the influence of many parameters like the porosity of the electrodes and the membrane properties. The main conclusions they reached are:

- Due to capillary forces, the liquid and the gas pressures are not in mutual equilibrium in the backing layer.

- The inefficiencies due to unreacted hydrogen or oxygen transport through the membrane are negligible
- At practical operating current densities, catalyst utilization is low.

While the limitations of their model are:

- It is valid only for fully hydrated membranes.
- It does not account for the drag force on water molecules.
- It is unable to predict flooding in the cathode backing layer due to water production.
- The polarization curve diverges from experimental data at high current densities.

In 1996, Weisbrod et al. [12] developed a one-dimensional steady-state isothermal model of a PEMFC that makes use of the Pseudo-homogeneous catalyst layers modeling approach. They have investigated the water balance in the backing layers and the influence of the catalyst layer thickness and platinum loading on the cell performance and the impact of the temperature and the cathode pressure on performance. Their main conclusion was that the cell performance passes through a maximum with respect to the platinum loading of the catalysts. One of the limits of their model is that, it neglects the kinetic resistance at the anode catalyst layer.

In 1998, Gurau et al. [13] developed a comprehensive two-dimensional steady-state Non-isothermal model of a PEMFC. They have studied in details the following points:

- The effect of the gas diffuser porosity on cell performance
- The effect of the inlet air velocity on cell performance.
- The oxygen concentration distribution at the gas channel/gas diffusion interface
- The effect of the oxygen concentration distribution on the operating current density
- The current density distribution at the membrane/cathode catalyst layer interface.

They found out that a non-uniform reactant distribution has an important impact on the current density. One of the very interesting things about their model is that, it is a

single or a unified domain model and thus it eliminated the need to arbitrary or inaccurate interfacial boundary conditions between the different fuel cell sandwich layers.

In 1998, Eikerling et al. [14] developed a one-dimensional steady-state isothermal model of a PEMFC.they have studied the effects of membrane parameters on cell performance and compared between a diffusion model and a convection model of the membrane. Their experimental data confirmed that water transport through the membrane is carried out by convection, for the most part. It should be noted however, that their model does not take into account the gas transport limitations in the electrodes and assumes that only the capillary forces affect the equilibrium water content in the membrane.

In 1999, Nguyen et al. [15] developed a two-dimensional steady-state isothermal model of a PEMFC.they investigated the effects of gas distributor design and the effects of electrodes dimensions on the cell performance. They reached the conclusions that the design of the gas distributor can reduce the gas diffusion layer thickness and that Diffusion plays an important role in the transport of oxygen to the reaction surface. However their model does not take into account the effects of the presence of liquid water.

In 2000, Um et al. [7] presented a comprehensive two-dimensional transient isothermal model of a PEMFC. Like Gurau et al., Um et al. used a unified single domain. The model accounts simultaneously for electrochemical kinetics, current distribution, hydrodynamics, and multicomponent transport. A single set of conservation equations valid for flow channels, gas-diffusion electrodes, catalyst layers, and the membrane region were developed and numerically solved using a finite-volume-based computational fluid dynamics technique. The numerical model was validated against published experimental data with good agreement. Subsequently, the model was applied to explore hydrogen dilution effects in the anode feed. The predicted polarization curves under hydrogen dilution conditions are in qualitative agreement with recent experiments reported in the literature. The detailed two-dimensional electrochemical and flow/transport simulations further revealed that in the presence of hydrogen dilution in the fuel stream, hydrogen is depleted at the

reaction surface, resulting in substantial anode mass transport polarization and hence a lower current density that is limited by hydrogen transport from the fuel stream to the reaction site. Finally, a transient simulation of the cell current density response to a step change in cell voltage was reported.

In 2001, Eaton, B.M., [16] developed a one-dimensional transient Non-isothermal model of a PEMFC. This model simulates only the membrane region and addresses important issues for the performance of the cell like the membrane water management and temperature distribution within the membrane. They reached the following conclusions:

- The higher the applied current density, the more water is driven from the anode to the cathode and out of the membrane.
- A positive pressure gradient between anode and cathode could be used to drive water towards the anode, hydrating it, since the anode side is more likely to dry out.

However, the inherent limitation of this model and the like is that it requires interfacial boundary conditions to be specified and some of these conditions might be arbitrary or even unrealistic.

In 2001, Genevey, D.B. [17] developed a one-dimensional transient Non-isothermal model of a PEMFC. This model simulates only the cathode catalyst layer region and investigates the effect of the membrane water content, temperature, porosity on the performance of the cell and addresses the mass transport limitations and flooding issues and the transient behavior of the catalyst layer. They reached the following conclusions:

- A higher porosity is favorable to oxygen diffusion and therefore, gives better performance. Smaller porosities affect both the oxygen concentration distribution and the current generation per unit volume distribution across the catalyst layer. Decreasing the porosity results in poorer performance.
- The catalyst loading can considerably increase the cell current density via an increased surface area. However, the effects of the catalyst surface area are limited by the oxygen transport resistance that occurs at high current densities.

- Though higher temperature is known to improve the cell performance, it has the opposite effects on the catalyst layer performance. The activation overpotential increases as the temperature increases and results in poorer performance of the catalyst layer.

Like M.Eaton et al. model, the inherent limitation of this model, is that it requires interfacial boundary conditions to be specified which might be arbitrary or even unrealistic. Another limitation is that, it does not take into account the concentration overpotential in computation of the polarization curves.

In 2002, Um et al. [18] developed a three-dimensional transient isothermal model of a complete PEMFC. The model incorporates the various modes of water transport; therefore it is able to provide comprehensive water management study, which is essential for PEM fuel cells in order to achieve high performance. The model is capable of simulating the fuel cell under a variety of reformate fuel for real life applications. The model is tested against available experimental data and previously published models. Since the model has been developed using the commercial software Fluent®, it can be easily applied for different flow field designs. Finally, the model is applied to several different operating conditions with different cell geometries and corresponding results are reported, including the effect of different flow field designs on cell performance.

In 2003, T.Berning et al. [19] developed a three-dimensional non-isothermal model of a PEMFC. They investigated in detail the effect of various operational parameters such as the temperature and pressure on the fuel cell performance. It was found that in order to obtain physically realistic results experimental measurements of various modeling parameters were needed. The results showed good qualitative agreement with experimental results published in the literature. In addition, the effect of geometrical and material parameters such as the gas diffusion electrode (GDE) thickness and porosity were investigated. The contact resistance inside the cell was found to play an important role for the evaluation of the impact of such parameters on the fuel cell performance.

Chapter Three
Mathematical Model

3.1 Overview of the model

Proton exchange membrane fuel cell (PEMFC) engines can potentially replace the internal combustion engine for transportation because they are clean, quiet, energy efficient, modular, and capable of quick start-up[7]. Since a PEMFC simultaneously involves electrochemical reactions, hydrodynamics, multicomponent transport, and heat transfer, a comprehensive mathematical model is needed to gain a fundamental understanding of the interacting electrochemical and transport phenomena and to provide a computer aided tool for design and optimization of future fuel cell engines. At high current densities of special interest to vehicular applications, excessive water is produced within the air cathode in the form of liquid, thus leading to a gas-liquid two-phase flow in the porous electrode [7]. The ensuing two-phase transport of gaseous reactants to the reaction surface, *i.e.,* the cathode/membrane interface, becomes a limiting mechanism for cell performance, particularly at high current densities (*e.g.,* >1 A/cm2) [7]. On the anode side, when reformate is used for the feed gas, the incoming hydrogen stream is diluted with nitrogen and carbon dioxide. The effects of hydrogen dilution on anode performance, particularly under high fuel utilization conditions, are significant. [20, 21].

The objective of this study is to develop a steady-state, two-dimensional model for electrochemical kinetics, and multicomponent transport in a realistic fuel cell and to develop an in-house CFD code based on the finite-volume method and use it in the investigation of the effect of the different operating conditions like temperature, pressure and reformate composition on the performance of the PEMFC. The CFD approach was first employed in electrochemical systems by [13] and has since been applied successfully to a variety of battery systems [7]. The following section describes a steady-state, two-dimensional mathematical model for electrochemical and transport processes occurring inside a PEMFC that is based on the previous work of Um et al. [7].

3.2 Numerical Model

Figure 3.1 schematically shows a PEMFC fuel cell divided into seven subregions: the anode gas channel, gas-diffusion anode, anode catalyst layer, ionomeric membrane, cathode catalyst layer, gas-diffusion cathode, and cathode flow channel. The present model considers the anode feed consisting of hydrogen, water vapor, and nitrogen to simulate reformate gas, whereas humidified air is fed into the cathode channel.

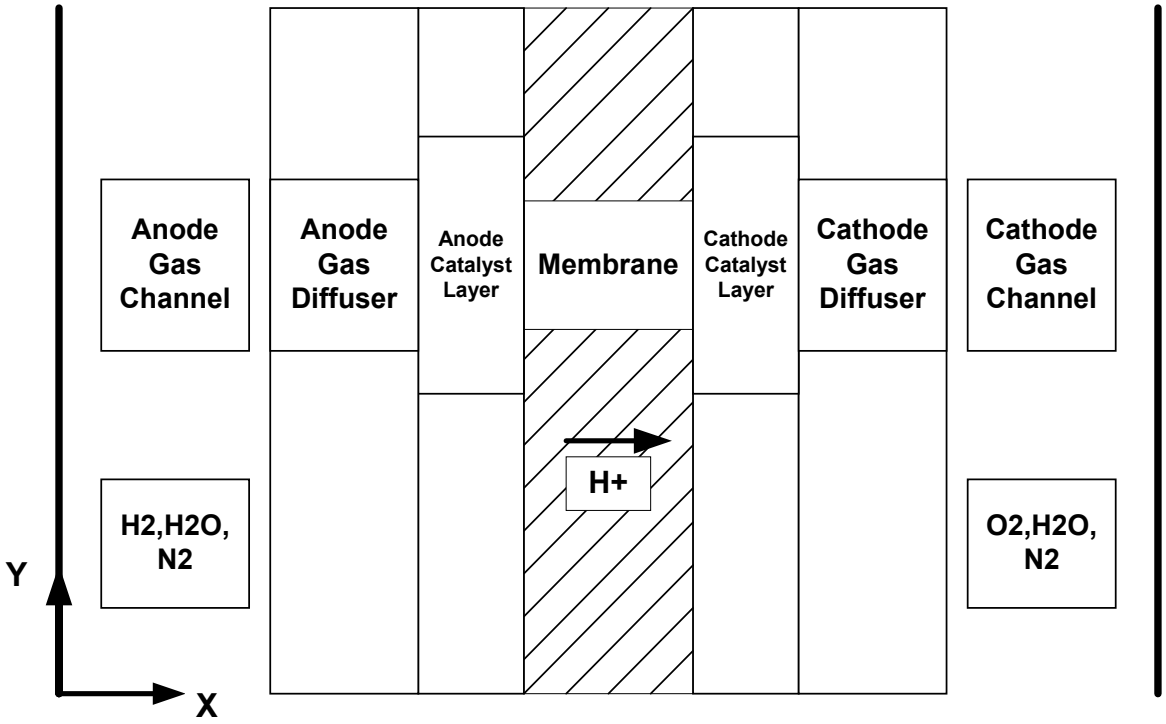

Figure 3.1 Schematic diagram of a proton exchange membrane fuel cell (PEMFC).

Hydrogen Oxidation and oxygen reduction reactions are considered to occur only within the active catalyst layers where Pt/C catalysts are homogeneously intermixed with the recast ionomer. The fuel and oxidant flow rates can be described by a stoichiometric flow ratio, ζ, defined as the amount of reactant in the gas feed divided by the amount required by the electrochemical reaction, That is:

$$\zeta_{+} = X^{\circ}_{O_2} \nu^{o}_{+} \frac{P_{+}}{RT} \frac{4F}{i\ A} \qquad (3.1)$$

$$\zeta_{-} = X^{o}_{H_2} \nu^{o}_{-} \frac{P_{-}}{RT} \frac{2F}{i\ A} \qquad (3.2)$$

where ν^{o} is the inlet volumetric flow rate to the gas channel, p and T the pressure and temperature, R and F the universal gas constant and Faraday's constant, I the current density, and A the electrode surface area. The subscripts (+) and (-) denote the cathode and anode sides, respectively. For convenience, the stoichiometric flow ratios defined in Eq. 3.1 and 3.2 are based on the reference current density of 1 A/cm², so that the ratios can also be considered as dimensionless flow rates of the fuel and oxidant [7].

3.3 Model assumptions.

This model makes the following assumptions:

(i) Steady-state.

(ii) Ideal gas mixtures.

(iii) Laminar flow due to small flow channels and low flow velocities.

(iv) Isotropic and homogeneous electrodes, catalyst layers, and membrane.

(v) Constant cell temperature.

(vi) Negligible ohmic potential drop in the electronically conductive solid matrix of porous electrodes and catalyst layers as well as the current collectors.

(vii) Electroneutrality. Which leads to the necessity of existence of a constant proton concentration throughout the membrane and catalyst layers and in concentration equal to the fixed charge concentration.

3.4 Governing equations

In this modeling work we took a single-domain approach for the governing differential equations by writing a single set of differential equations that is valid for all the sub-regions instead of writing separate sets of differential equations for different sub-regions, As a result, no interfacial conditions are required to be specified at internal boundaries between various regions. Generally, fuel cell operation under isothermal conditions is described by mass, momentum, species, and charge

conservation equations. Thus, under the above-mentioned assumptions, the model equations can be written, as:

Mass	$\nabla.(\varepsilon\ \rho \mathrm{u}) = 0$	(3.3)
Momentum	$\nabla.(\varepsilon\ \rho \mathrm{uu}) = -\varepsilon \nabla P + \nabla.(\varepsilon\mu\ \ \nabla u) + \mathrm{S_u}$	(3.4)
Species	$\nabla.(\varepsilon\ \rho \mathrm{uY_k}) = \nabla.(\rho D_k^{\ eff} \nabla Y_k) + \mathrm{S_k}$	(3.5)
Charge	$\nabla.(\sigma_e\ \nabla \Phi_e) + \mathrm{S}_\phi = 0$	(3.6)

Here, **u**, p, $\mathrm{Y_K}$, and Φ_e denote the fluid velocity vector, pressure, mass fraction of chemical species k, and the phase potential of the electrolyte membrane, respectively. The diffusion coefficient of species k in Eq. 3.5 is an effective value modified via the so-called Bruggman correlation to account for the effects of porosity in porous electrodes, catalyst layers, and the membrane. That is:

$$D_k^{eff} = \varepsilon^{1.5} D_k \qquad (3.7)$$

Where ϵ is the porosity of the relevant porous region. The three source terms, $\mathrm{S_u}$, $\mathrm{S_k}$, and S_ϕ, appearing in momentum, species, and charge conservation equations represent various volumetric sources or sinks arising from each sub-region of a fuel cell. Detailed expressions of these source terms are given in Table 3.1. Specifically; the momentum source term is used to describe Darcy's drag for flow through porous electrodes, active catalyst layers, and the membrane. In addition, electro-osmotic drag arising from the catalyst layers and the membrane is also included. Either generation or consumption of chemical species k and the creation of electric current (see Table 3.1) occurs only in the active catalyst layers where electrochemical reactions take place. The $\mathrm{S_k}$ and S_ϕ terms are therefore related to the transfer current between the solid matrix and the membrane phase inside each of the catalyst layers. These transfer currents at anode and cathode can be expressed as follows [22]:

$$j_a = a\ j_{o,a}^{ref}\left(\frac{C_{H2}}{C_{H2,rec}}\right)^{\gamma_{H2}}\left(\frac{\alpha_a + \alpha_c}{\overline{R}\,T}.F.\eta(x,y)\right) \quad (3.8)$$

$$j_c = -\,a\ j_{o,c}^{ref}\left(\frac{C_{O2}}{C_{O2,rec}}\right)^{\gamma_{O2}}\exp\left(-\frac{\alpha_c}{\overline{R}\,T}.F.\eta(x,y)\right) \quad (3.9)$$

Table 3.1. Source terms for momentum, species, and charge conservation equations in the various sub-regions.

	S_u	S_k	S_Φ
Gas Channels	0	0	N/A
Gas Diffusion Layer	$-\frac{\mu}{K}\varepsilon u$	0	0
Catalyst Layers	$-\frac{\mu}{k_p}\varepsilon_m\varepsilon_{mc}u + \frac{k_\phi}{k_p}z_f c_f F\nabla\Phi_e$	$\begin{cases} -\frac{j_a M_{H2}}{2F} \text{ for } H_2 \\ \frac{j_c M_{O2}}{4F} \text{ for } O_2 \\ -\frac{j_c M_{H2O}}{2F} \text{ for } H_2O \end{cases}$	j
Membranes	$-\frac{\mu}{k_p}\varepsilon_m u + \frac{k_\phi}{k_p}z_f c_f F\nabla\Phi_e$	0	0

Where the surface overpotential, $\eta(x, y)$, is defined as:

$$\eta(x,y) = \Phi_s - \Phi_e - V_{oc} \quad (3.10)$$

Where Φ_s and Φe stand for the potentials of the electronically conductive solid matrix and electrolyte, respectively, at the electrode/ electrolyte interface. V_{oc} is the open-circuit potential of an electrode. It is equal to zero on the anode but is given by the Nernst equation [23] on the cathode, namely:

$$V_{oc} = 1.229 - 0.83\times10^{-3}\,(T - 298.15) + 4.31\times10^{-5}\,T\,[\ln p_{H_2} + \frac{1}{2}\ln p_{O_2}] \quad (3.11)$$

Where T is in Kelvin and V_{oc} is in volts. Examination of Eq. (3.11) shows a decrease of the open circuit voltage with temperature in contrast with the experimental

measurement [13] and accordingly, the result of the experiment in [24] has been used for the effect-of-temperature simulation, namely:

$$V_{oc} = 0.0025\,T + 0.2329 \qquad (3.12)$$

Based on the experimental data of [24] the dependence of the cathodic exchange current density on temperature can be fitted as:

$$\frac{i_o(T)}{i_o(353K)} = \exp\left(0.014189(T-353)\right) \qquad (3.13)$$

Based on an order-of-magnitude analysis of the experimentally determined values of [24] and the values used by [23] the cathodic exchange current density has been assumed to vary logarithmically with the cathode pressure according to:

$$a\, j_{o,c}^{ref} = (3106.7\,Ln(P_{cathode})) - 34767. \qquad (3.14)$$

where the reference exchange current density times the catalyst specific surface area $a\, j_{o,c}^{ref}$ is in units of A/m^3 and the cathode pressure $P_{cathode}$ is in Pa. although it might appear somewhat arbitrary but it has to be kept in mind that at this stage of the analysis, the main objective is to qualitatively understand the impact of the cell pressure on the different cell parameters and to represent it as closely as possible.

Under the assumption of a perfectly conductive solid matrix for electrodes and catalyst layers, Φ_s is equal to zero on the anode side at the anodic current collector and to the cell voltage on the cathode side at the cathodic current collector[7]. The species diffusivity, D_K, varies in different subregions of the PEMFC depending on the specific physical phase of component k. In flow channels and porous electrodes, species k exists in the gaseous phase, and thus the diffusion coefficient takes the value in gas, whereas species *k* is dissolved in the membrane phase within the catalyst layers and the membrane, and thus takes the value corresponding to dissolved species, which is usually a few orders of magnitude lower than that in gas. In addition, the diffusion coefficient is a function of temperature and pressure [25] *i.e.*

$$D(T) = D_o\left(\frac{T}{T_o}\right)^{3/2}\left(\frac{P_o}{P}\right) \qquad (3.15)$$

The mixture local density (ρ) is given for multi-component system as:

$$\rho = \frac{P}{RT} \tag{3.16}$$

Where R is the local gas constant for the local gas-mixture defined as:

$$\mathrm{R} = \frac{\overline{R}}{M} \tag{3.17}$$

Where $\overline{R}$ the universal gas constant and M is the molecular weight of the local gas mixture, which is calculated through the use of the following formula:

$$M = \frac{1}{\sum \frac{y_k}{M_k}} \tag{3.18}$$

Where the sum is taken over all the locally existing gases comprising the mixture. Like [26] the mixture local viscosity is calculated using a mass-weighted mixing law which reads:

$$\mu = \sum Y_k \, \mu_{\mathrm{k}} \tag{3.19}$$

Where Y_k is the species mass fraction and the sum is to be taken over all the locally existing gaseous components comprising the mixture.

In order to closely match the experimental polarization curves of Ticianelli et al.[27] the Protonic conductivity was taken to be 6.8 S/m at 80 °C and 6.2 S/m at 50 °C and then a linear scaling with temperature was used to estimate its value at other temperatures. We finally reached the following formula:

$$\sigma_e(T) = 0.02T - .26 \tag{3.20}$$

Where the temperature is in K and the membrane conductivity is in S/m. This approach of adjusting the value of the protonic conductivity has been followed by [28] and [19] where [28] used a constant value of 7 S/m which is very close to the value used in this work at 80 °C.

For this multicomponent system, the general species transport equation given in Eq. 3.5 is applied to solve for mole fractions of hydrogen, oxygen, and water vapor. The

mole fraction of nitrogen is then obtained by subtracting the sum of the species mole fractions from the unity. Once the electrolyte phase potential is determined in the membrane, the local current density along the axial direction can be calculated as follows:

$$i(y) = -\sigma_e^{eff} \left. \frac{\partial \Phi_e}{\partial x} \right|_{x=I.F.} \qquad (3.21)$$

I.F. means the interface between the membrane and cathode catalyst layer. The average current density is then determined by:

$$\mathrm{i}_{\mathrm{avg}} = \frac{1}{\mathrm{L}} \int_0^{\mathrm{L}} i(y)\, \mathrm{dy} \qquad (3.22)$$

Where *L* is the cell length.

3.5 Boundary conditions.

Equations 3.3 -3.6 form a complete set of governing equations for (*m* + 5) unknowns, where *m* is the physical dimension of the problem: $U, V, P, Y_{H2}, Y_{O2}, Y_{H2O}, and\ \phi_e$. Their boundary conditions are required only at the external surfaces of the computational domain due to the single-domain formulation used.

- .At the fuel and oxidant inlets, the following conditions are prescribed.

$$V_{in,anode} = V_-\ ,\ \mathrm{V}_{\mathrm{in,cathode}} = V_+ \qquad (3.23)$$

$$U_{in,anode} = U_-\ ,\ \mathrm{U}_{\mathrm{in,cathode}} = U_+ \qquad (3.24)$$

$$Y_{H2,anode} = Y_{H2-}\ ,\ Y_{H2\,in,anode} = Y_{H2+} \qquad (3.25)$$

$$Y_{O2,anode} = Y_{H2-}\ ,\ Y_{O2\,in,anode} = Y_{O2+} \qquad (3.26)$$

$$Y_{H2O,anode} = Y_{H2O-}\ ,\ Y_{H2O\,in,anode} = Y_{H2O+} \qquad (3.27)$$

- For $Y_{H2}, Y_{O2}, and\ Y_{H2O}$ the remaining boundary conditions are, no-flux conditions everywhere along the boundaries of the computational domain except at the inlets and outlets of the gas channels

- At the outlets of the gas channels the species concentration fields were assumed to be fully developed.
- Initial calculations of the pressure drop along the gas channels revealed that it is negligible and accordingly we chose to use the constant pressure boundary condition at the exit of the gas channels rather than the fully developed one since the former is generally known to yield better convergence rates [29].
- The boundary conditions for the electrolyte phase potential ϕ_e are no-flux everywhere along the boundaries of the computational domain, which –in this case- is the catalyst layers and the electrolyte membrane. It is to be noted that the potential is constant along the gas diffuser layers as we neglected their resistance in this model and also that the electrolyte phase potential equation is not applicable throughout the gas channels.

Chapter Four

Numerical-solution

4.1 Introduction

Numerical codes offer a cost effective alternative to experiments. However the accuracy of the numerical code must be assured. This can be accomplished by two ways: verification and validation. Verification involves ensuring that the differential and algebraic equations are correctly formulated and properly solved. Validation involves ensuring that the numerical code provides the correct solution. Validation of the code against experiments assures the closeness by which the mathematical model resembles the physical phenomena being simulated.

This chapter describes in details the CFD code that has been developed for the problem at hand.

4.2 Description of the TEAM CFD code

The finite volume method was originally developed as a special finite difference formulation. The numerical algorithm in this method could be best summarized as follows [30]:

- Formal integration of the governing equations over all the finite control volumes of the solution domain.
- Discretization involves the substitution of a variety of finite-difference-type approximations for the terms in the integrated equation representing flow processes such as convection, diffusion and sources. This converts the integral equations into a system of algebraic equations.
- Solution of the algebraic equations by an iterative method.

TEAM is a computer code based on the finite volume method, for simulation of steady two-dimensional, turbulent elliptic flows. The code can be applied to plane and

axi-symmetric flows. This program uses quadratic interpolation (Quick) or power law interpolation (PLDS) to discretize the convective terms of the governing equations, and it has the option of either using the SIMPLE Algorithm or the PISO Algorithm for velocity-pressure coupling. The program although primarily meant for turbulent flows, solves laminar flow as well. The code structure is very transparent allowing considerable flexibility for adaptation to the varying flow situations.

In this chapter, we will gloss over the original TEAM code structure, including description of the standard case built in it. Then proceed to summarize the modifications that were required for adaptation of the code to the problem at hand.

4.3 Overall structure

TEAM is divided into two major parts; the user area and the general area. The user area consists of two routines, the main routine TEAM and subroutine user.

The general area consists of subroutines for equations (CALC`S), the TDMA solver (LISOLV), the printing routine (PRINT) and the subroutine which produces the geometrical quantities and initial values. Overall control and communication among subroutines is shown in the flow chart in appendix A. TEAM, the main routine is the communication center of the program. It controls the interlinkage among subroutines and the sequence of operations. This is done by following a set of call statements to subroutines related to the problem of interest. The sequence starts with a call to SET in the user. Subroutine to define the problem dependent variables and follows by two calls to GRID and INLET in the user subroutine to set up control volume faces and inlet conditions respectively. After a call to OUTPI in USER to produce initial output (title, geometrical information, initial conditions etc.), a sequence of CALLS to CALC`S in the general area is executed. When the convergence criteria are satisfied, CALL to OUTP in USER area is made to produce the final output [30].

4.4 Solution Algorithm

The main solution steps can be summarized as follows:

1. Initialize the variable field U*, V*, P*, K* and E*.
2. Calculate the effective transport coefficients.
3. Assemble the coefficients for the U-momentum equations.
4. Impose the boundary conditions by modifying the coefficients and sources.
5. Solve for the U-field.
6. Similarly, solve for V-field.
7. Similarly, solve for $P1^{'}$.
8. Adjust velocities.
9. Update pressure then go to step 12 ← SIMPLE
10. Solve for $P_2^{'}$. ← PISO
11. Update pressure.
12. Follow steps similar to steps 3 through 5 to solve for K and ε.
13. Repeat steps 2 through 12 until the specified convergence criteria are reached.

4.5 Standard TEAM case

This case consists of uniform turbulent circular jet impinging on a plate held normal to the discharge. The geometry is shown in figure 4-2.

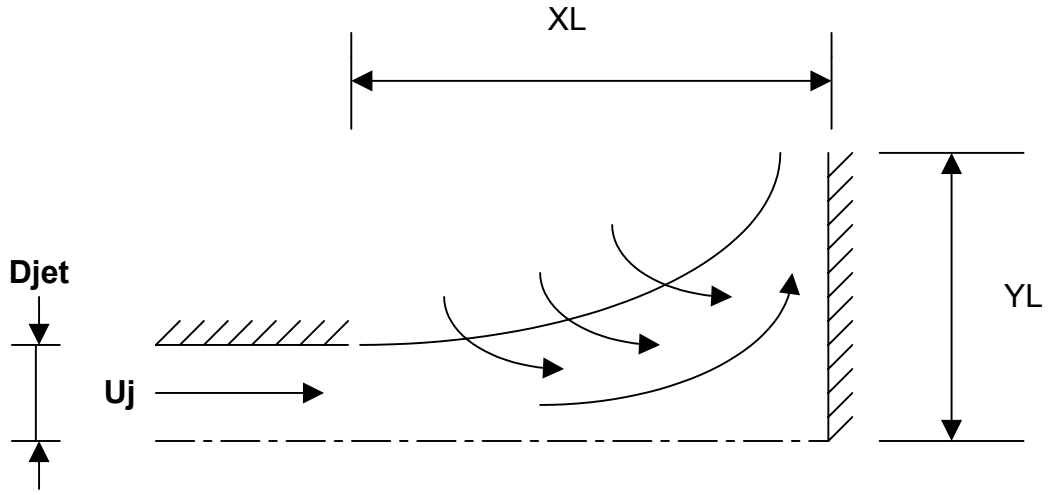

Fig.4.1 Turbulent impinging circular jet

Since it deals with turbulent flow, turbulent viscosity of the K and ε equations need to be updated in each iteration. A 15 x 15 non-uniform mesh is used in this case; in the X-direction the grid lines expand from both left and right boundaries with expansion ratios of RAXL and RAXR, respectively; in the Y-direction the grid lines expand from the edge of the jet, DJET, to the top and bottom boundaries with expanding rates of RAY and RAJET, respectively [31].

4.6 Main code modifications

In order to adapt the TEAM code to the problem at hand, the following list of modifications were needed:

1. Deactivation of the $k-\varepsilon$ Turbulence model.
2. Designing the fuel cell grid.
3. Addition of three subroutines, namely CALCYO2, CALCYH2, CALCYH2O to solve the species conservation equations for oxygen, hydrogen and water vapor respectively.
4. Addition of subroutine, namely CALCPH to solve the electrolyte phase potential equation.
5. Porous media correction of the conservation equations.
6. Modification of the boundary conditions.
7. Updating the local mixture density and viscosity.
8. Addition of subroutine namely CALCIAVG to evaluate the cell average current density whenever convergence is reached.

4.7 The VTC Numerical Solution Algorithm

A Voltage-to-current (VTC) numerical algorithm has been developed. The Algorithm enables prediction of the cell current density based on a desired input cell voltage. The solution starts by specifying the cell operating conditions namely pressures, velocities, temperature, and cell voltage. The code then proceeds to solve the overall mass conservation, momentum equations then solves the species equations for O_2, H_2

and H_2O and finally the electrolyte phase potential equation, after each iteration the code locally updates the mixture density ,viscosity and source terms until convergence criteria are met. Upon reaching convergence, the code proceeds to calculate the cell average current density. The VTC algorithm is summarized in appendix B. In order to implement this algorithm the original TEAM code needed some modifications which will be discussed in the next sections.

4.8 Code modifications

Detailed explanation of the modifications made to the original TEAM code will be presented in the following sub-sections.

4.8.1 Deactivation of k-ε turbulence equations

Since the flow in our problem is inherently laminar because of small flow channels and low flow velocities, we had deactivated the $k-\varepsilon$ turbulence equations.

4.8.2 Grid Layout

In order to better depict the phenomena occurring in the catalyst layers, the grid has been designed as a non-uniform 36×138 staggered grid in which the cells have been clustered within the anode and cathode catalyst layers. The fuel cell grid is shown below in fig. 4.4. In the design of the above grid, we have limited the cell expansion ratios in both the X and Y directions to a value of 1.1 to avoid the ensuing numerical instabilities resulting from the big truncation errors [29]. The expansion or contraction in the cell size has been assumed to follow a geometric series having a common ratio of 1.1.

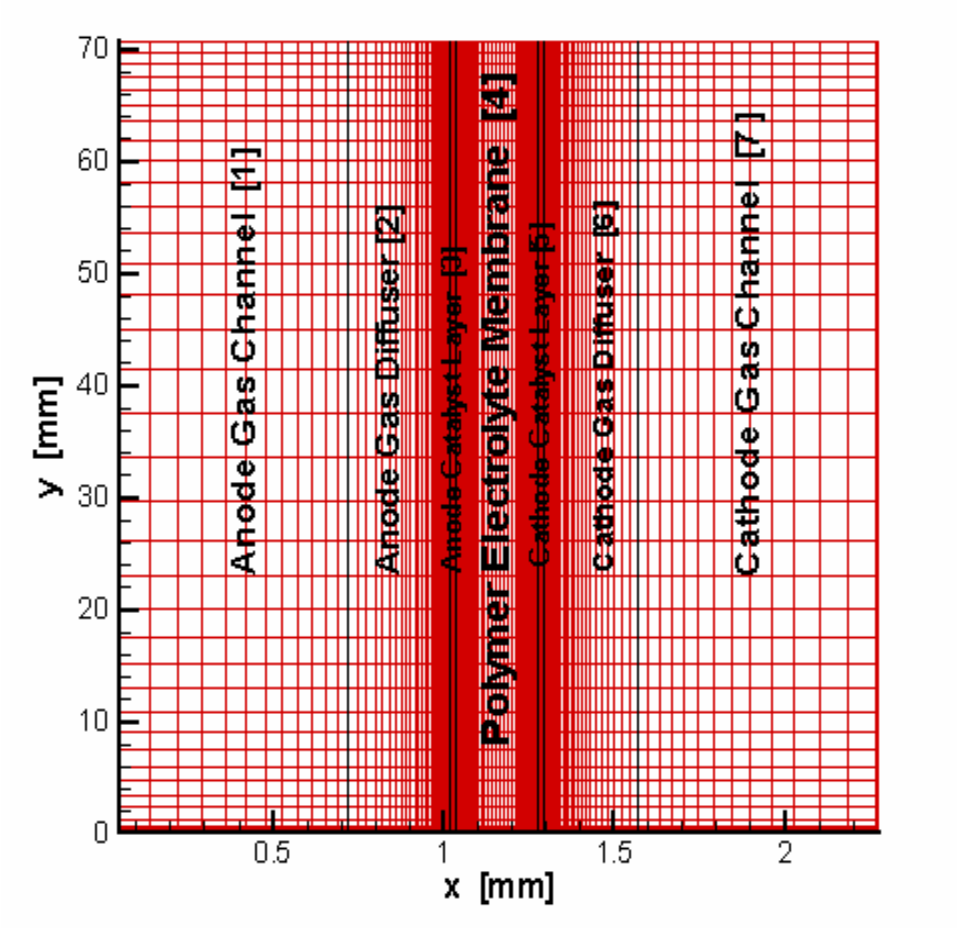

Fig.4.2 PEMFC grid

4.8.3 Species conservation equations

In principle, the mechanisms governing the species transport are very much like the mechanisms governing the energy transport. This naturally-forthcoming similarity could be readily understood upon consideration of the steady-state formulation of the species conservation equation and the energy equation namely:

$$\nabla.(\rho\vec{V}h) = \nabla.(K\nabla T) + S_h \qquad (4.1)$$

$$\nabla.(\rho\vec{V}Y_k) = \nabla.(\rho D_k \nabla Y_k) + S_k \qquad (4.2)$$

Careful consideration of the two equations reveals this inherent similarity between them. In the original code, there were three embedded scalar subroutines Viz, the energy equation subroutine, the K-subroutine and the ε subroutine and they are all very much alike so that all that was required is just to define the new diffusive

transport coefficient for species equations i.e. the diffusion coefficient D_k times the mixture density ρ for each species.

4.8.4 Electrolyte phase potential equation

The equation for electrolyte phase potential reads

$$\nabla.\sigma_e \nabla \phi_e + S_\phi = 0 \qquad (4.3)$$

Careful consideration of these equations reveals that, the electrolyte phase potential is transported only through the diffusive and source terms and that there are no convective terms. Consequently the skeleton scalar equations embedded in the code were modified to nullify the mass flow rate through the different cell faces and accordingly the connective coefficients reduce to zero so that all that remain are the diffusive plus the source terms.

4.8.5 Porous media correction

Consideration of the continuity and momentum equations through porous media reveals the analogy between the continuum and porous media flow equations. for porous media there only appears an additional sink term namely:

$$S_u = \frac{-\mu}{K} \varepsilon \vec{u} \qquad (4.4)$$

That effectively simulates the porous media flow through acting as a sink bringing about a very large pressure drop and thus , substantially reducing the flow velocity within the pores of the porous media.

This source term has been inserted in the U and V momentum equations as:

$$SPU = \frac{-\mu}{K} \varepsilon \times Cell \text{ Volume} \qquad (4.5)$$

$$SPV = \frac{-\mu}{K} \varepsilon \times Cell \text{ Volume} \qquad (4.6)$$

It is to be noted that the porosity need not be referenced anymore either in the pressure correction or in the species equations since its effect will be fed back through the substantial drop in the flow velocity within the pores, and this is guaranteed by the

source terms appearing in the momentum equations. However the velocities thus obtained are reduced velocities defined as:

$$u = \frac{u_{Da}}{\varepsilon} \qquad (4.7)$$

Where u_{Da} is the Darcy velocity [32]. By virtue of the above formulation, the same code used for continuum could be readily used for porous media flows.

4.8.6 Modification of the boundary conditions

The boundary conditions that were used in the previous chapter have already been mentioned. Those B.C.s have been inserted into the entries MODU, MODV, MODP, MODYO2, MODYH2, MODYH2O, and MODPH.

For freezing the species mass fractions through some regions of the domain the source term of the relevant species was assigned a sufficiently large value that effectively froze the species mass fractions to the required value (zero in our case) according to [30] and [33] the linearized source term form reads:

$$S = S_U + S_P \phi_P \qquad (4.8)$$

By letting $S_P = -GREAT, \mathrm{S_U} = GREAT \times \phi_{fix}$

Where GREAT is a sufficiently large value and ϕ_{fix} is the value of ϕ to be fixed (zero in our case) at the relevant grid node(s).

4.8.7 Updating the local mixture density and viscosity

Use has been made of the ideal-gases mixture equation of state (Eq.3.16) to calculate the local mixture density. Whereas the mixture local viscosity was calculated using a mass-weighted mixing law (Eq.3.19).

Once the species mass fractions are calculated the local mixture density and viscosity are corrected and used for the subsequent iterations.

Worthy of mentioning here is the fact that equation 3.16 does not hold throughout the catalyst layer-membrane region since the reactants dissolve in the water at the interface and are then carried to the reaction sites[13]. However at this stage of the current modeling frame-work this phenomenon will be neglected and the assumption that they are transported as components of the gas mixture will be made.

The above equations were inserted into the subroutine PROPS which is invoked each iteration to update the local mixture density , viscosity, and the diffusivities of the mixture components.

4.8.8 Average current density subroutine

This subroutine calculates the average current density by numerical integration of the electrolyte phase potential gradient along the cathode catalyst layer-membrane interface through application of Eq.3.21 to calculate the local current density along the interface and then by application of Eq.3.22 to calculate the average current density. This integration has been performed using the trapezoidal rule.

4.9 Convergence criteria

For the present 138×36 mesh, the coupled set of equations was simultaneously solved, and the solution was considered to be convergent when the relative error in each field between two consecutive iterations was less than 10^{-6}. A typical simulation involving approximately 35,000 unknowns required about 3 minutes of central processing unit time on a 2 GHz PC.

4.10 Running the PEMCU Code

In the previous subsections the main modifications of the original TEAM code which lead to the development of the new PEMCU code have been illustrated. Appendix C describes the flow-chart of the new PEMCU code.

The PEMCU code requires specification of the cell operating conditions viz. voltage, temperature, pressure, stoichiometric flow ratios, relative humidity of the feed streams, oxygen to nitrogen inlet percent and the hydrogen to nitrogen inlet percent. Once those conditions are specified the code does not require any extra input or calculations on the part of the user.

Chapter Five
Results and Discussion

5.1 Model validation

A systematic comparison with the experimental results is not possible at this stage, mainly due to the absence of well-established, benchmark data. Nevertheless, comparisons of the present numerical model were made to the experimental data of Ticianelli *et al.*[27] for a single cell operated at two different temperatures. The exact experimental conditions of [27] were incompletely reported. The base-case parameters employed in the following simulations are listed in Appendix D.

5.1.1 Effect of Temperature

In order to successfully model the effect of the temperature on the fuel cell performance, a basic understanding of its direct influence on various model parameters is required. The properties most dependent on temperature are:

- The composition of the incoming gas streams. The partial pressure of water vapor entering the cell depends on the temperature only. Thus, the molar fraction of water vapor is a function of the inlet pressure and temperature, and so the molar fraction of the incoming hydrogen and oxygen depend on the temperature and pressure as well.
- The exchange current density of the oxygen reduction reaction (ORR) increases rapidly with temperature due to the enhanced reaction kinetics. Use has been made of the correlation obtained experimentally by [24].
- The membrane conductivity σ_e increases, because a higher temperature leads also to a higher diffusivity of the hydrogen protons in the electrolyte membrane, thereby reducing the membrane resistance. Use has been made of a linear fit of the membrane protonic conductivity with temperature.

- The diffusivities of the gas mixture components increase as the temperature increases according to the relation. (3.15).

Taking into account the variation of all the above-mentioned parameters is the basis of the simulations that have been made. Figure 5.1 compares the polarization curves obtained from the present numerical solution to the measurements of [27] at 80 °C and 50 °C.

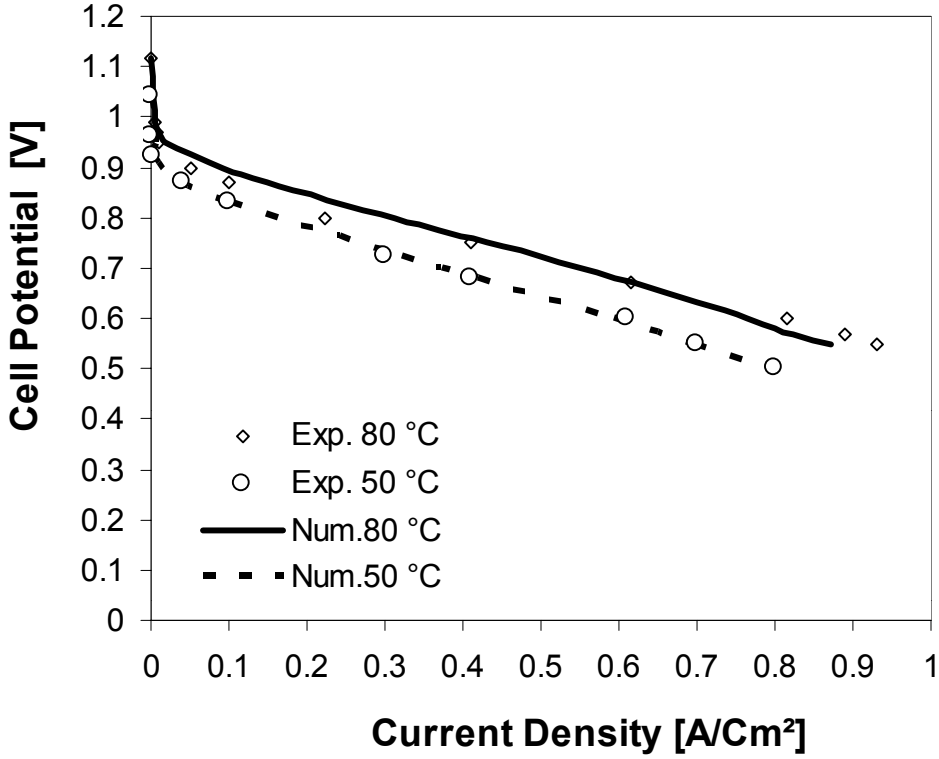

Fig.5.1 Comparison of predicted and measured cell polarization curves
[Base case conditions]

The computed curves show close agreement with the experimental data however quantitative comparison of the results is not possible due to the lack of specific information about the conditions of this experiment.

A series of runs were then made for the practical range of the cell operating temperatures i.e. 50 °C to 100 °C. It was found -as evidenced by Fig.5.2- that increasing the operating temperature leads to improved cell performance in terms of the cell characteristic polarization curve because of the reduced cell internal resistance-that is dominated by the polymer electrolyte membrane resistance- reduced

activation overpotential and overall improvement in the mass transport to the reaction sites.

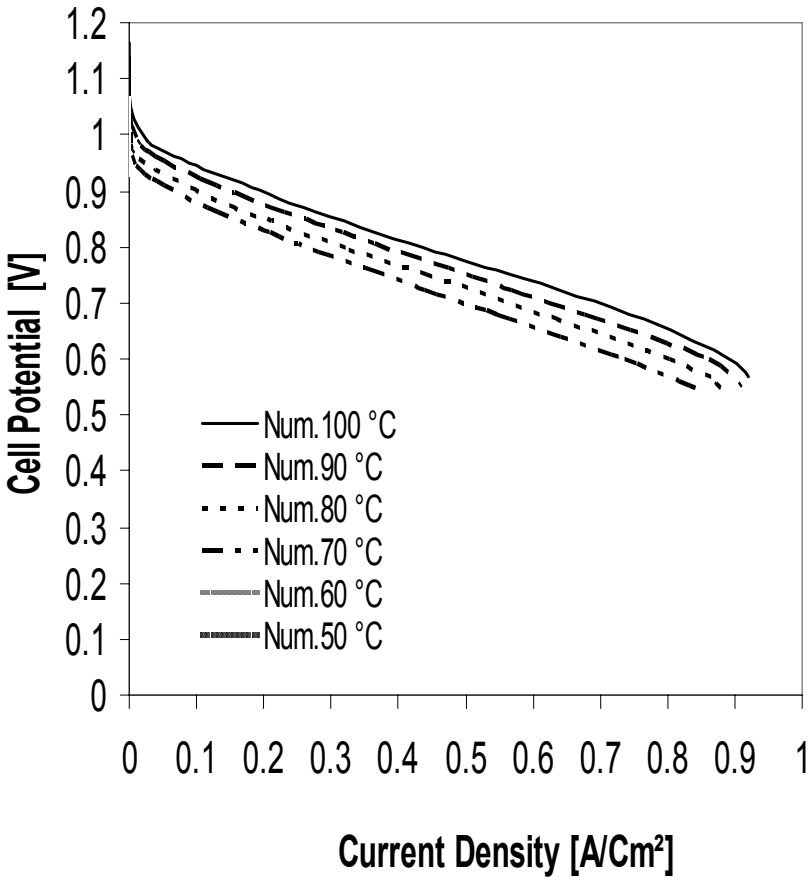

Fig. 5.2 Computed Polarization curves at different operating temperatures [Base case conditions]

However increasing the operating temperature is limited by the high vapor pressure of the water in the ion exchange membrane which leaves the membrane susceptible to dehydration and subsequent loss of ionic conductivity [1] and also by the maximum temperature that the polymer membrane can withstand which is about 80 °C [17].

5.1.2 Effect of Pressure

Similar to the temperature, the operating pressure affects numerous parameters that are important for the fuel cell operation, among which are:

- The inlet gas compositions.
- The exchange current density of the oxygen reduction reaction. Use has been made of Eq.3.14.
- The diffusivities of the gas mixture components decrease as the pressure increases According to the relation (3.15). Hence, a doubling of the pressure will cut the binary diffusivity in half.

Again, a detailed comparison with experimental results from the literature can only be made on a qualitative basis, since the exact conditions of the various experiments are not reported. In a like manner, the operating pressure was found to impact the fuel cell performance.

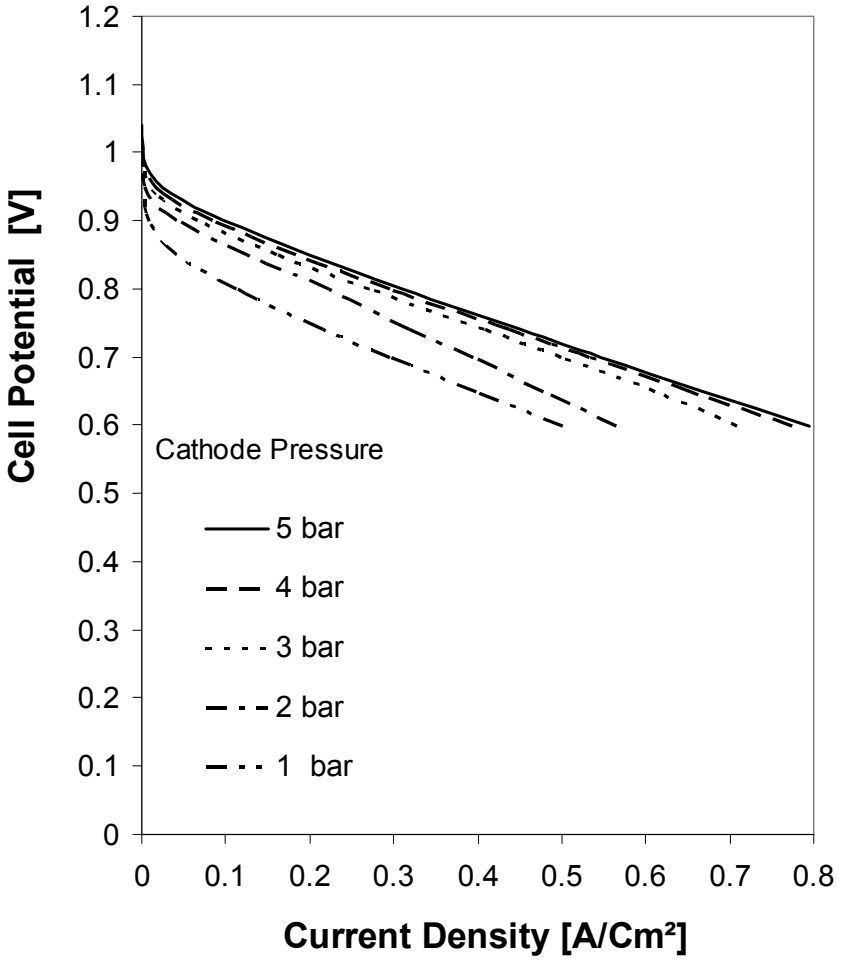

Fig.5.3 Effect of the operating pressure on the cell performance

[Base case conditions, Anode pressure=1bar]

It was found that increasing the cathode pressure improves the polarization curve of the cell up to a certain limit (3 bar) beyond which any further increase in the cathode pressure does not lead to a significant improvement in the performance (as shown in Fig.5.3) and may not counterbalance the required pumping power of the cathode stream. And thus, may not be justified. This is in agreement with the recent numerical predictions of [19] and the measurements of Kim et al. [34].

5.1.3 Fuel cell hydrodynamics

Due to the assumption of laminar flow in the gas channels, one should expect a fully developed parabolic velocity profile in the gas channels with vanishing velocities at solid walls (no slip condition).this is clear in fig.5.4 where the velocity vector plot has been drawn throughout the fuel cell.

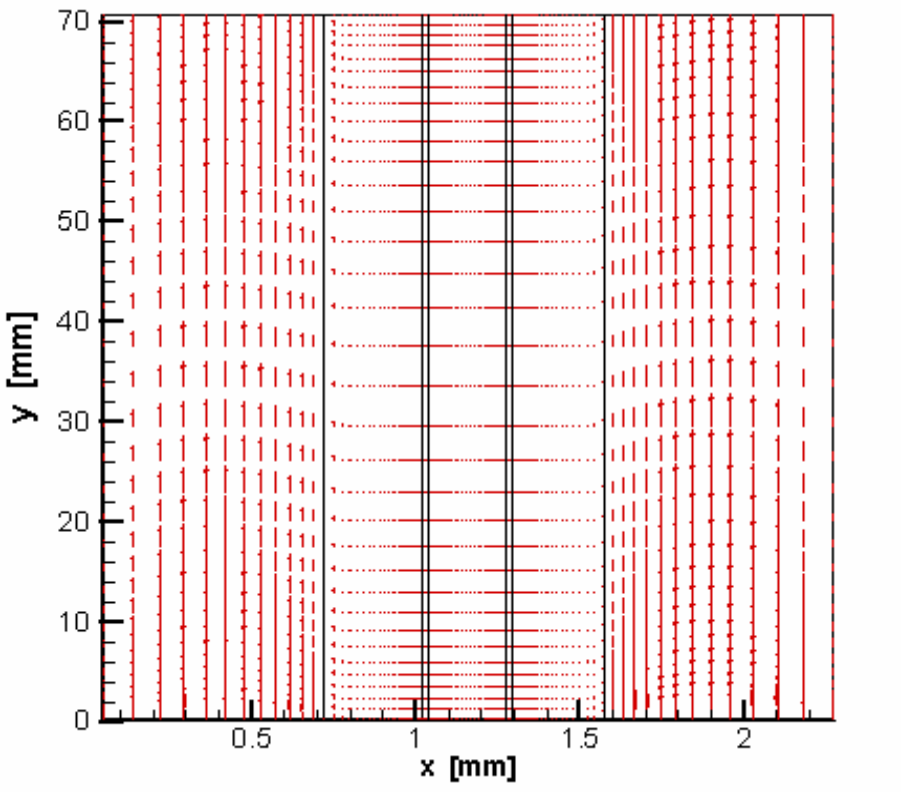

Fig.5.4 Velocity vector plot throughout the cell
[Base case conditions]

Fig.5.5 below shows the predicted velocity profile in the anode gas channel for an inlet velocity of 0.157 m/s (at V=0.6 Volt, T=353 K) It was found to exactly mimic the velocity profile predicted by [13] that is shown in fig 5. 6. A very prominent common characteristic of the two predicted velocity profiles is that their maximum value does not lie on the center line of the gas channel but is rather shifted towards the adjacent porous medium by about 3 % of the gas channel width (the same value predicted by [13]). At the gas channel wall the velocity is essentially zero (no slip) while at the porous medium-gas channel interface the velocity acquires a non-zero value which is in agreement with [35] and [13] as shown in fig5.6.

The macroscopic velocity in the porous medium drops very fast from the interface with the channel in a very thin layer of the order of the pore size ~0.06 mm which is quite in good agreement with the values predicted by [36] and [13].

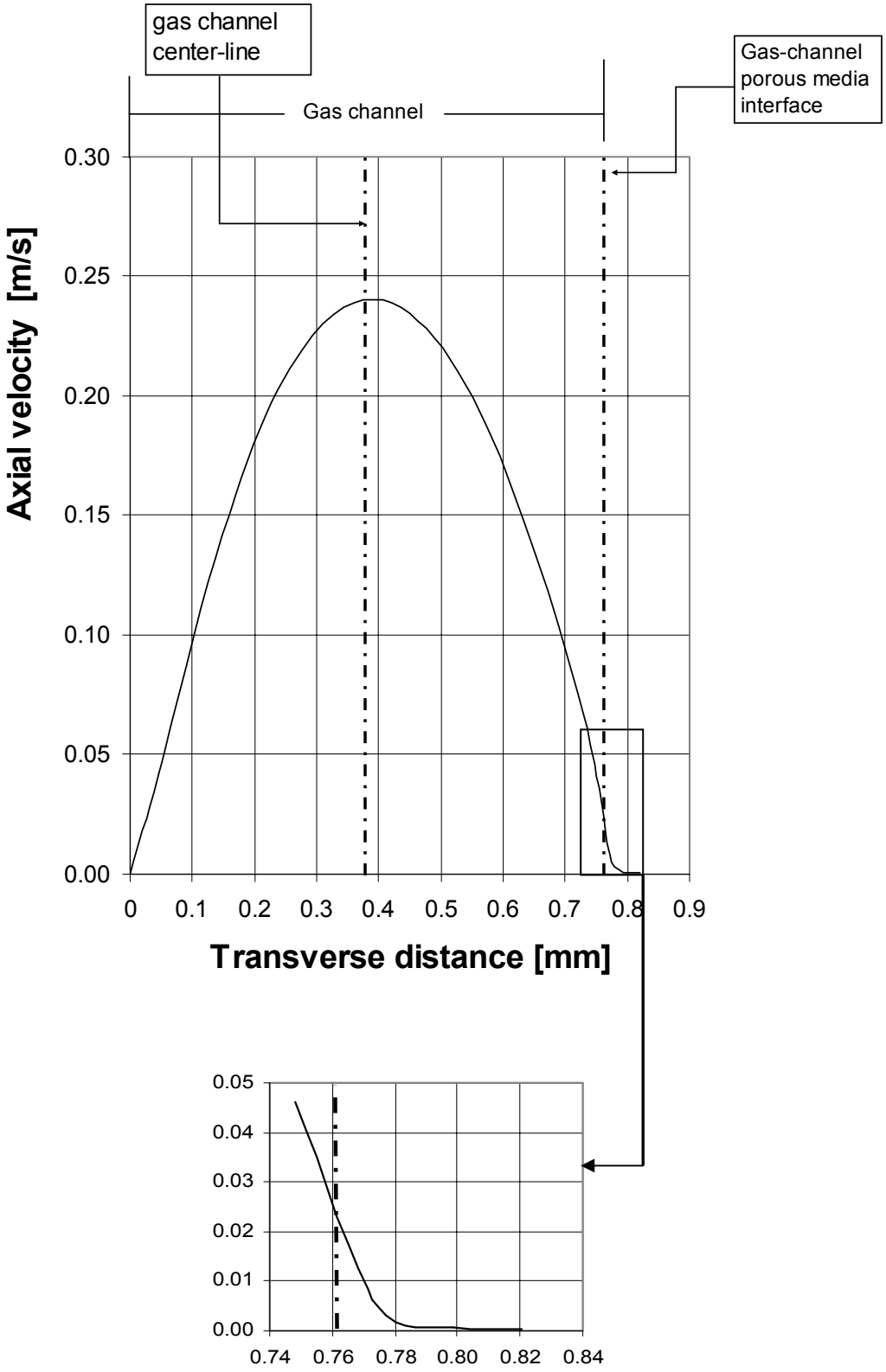

Fig.5.5 Computed Axial velocity profile across the channel gas diffuser domain at Y=4.5 cm [Base case conditions]

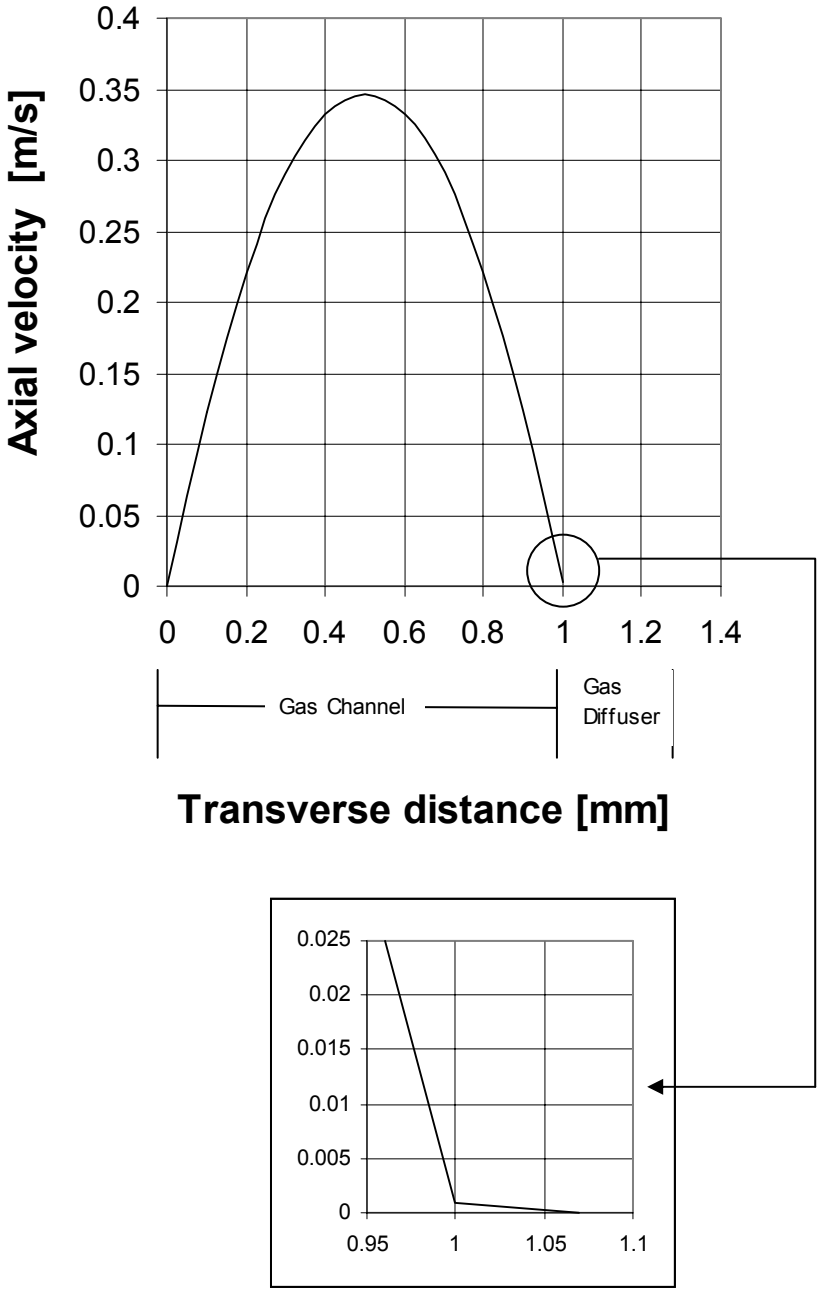

Fig.5.6 Velocity Profile across the gas-channel gas-diffuser domain at some distance from the inlet, adapted from [13]

The pressure field also showed similar characteristics as those predicted by [35] and [13]. With a constant axial pressure gradient and the absence of transverse pressure gradient in the coupled gas channel-gas diffuser sub-domain as shown in fig5.7.

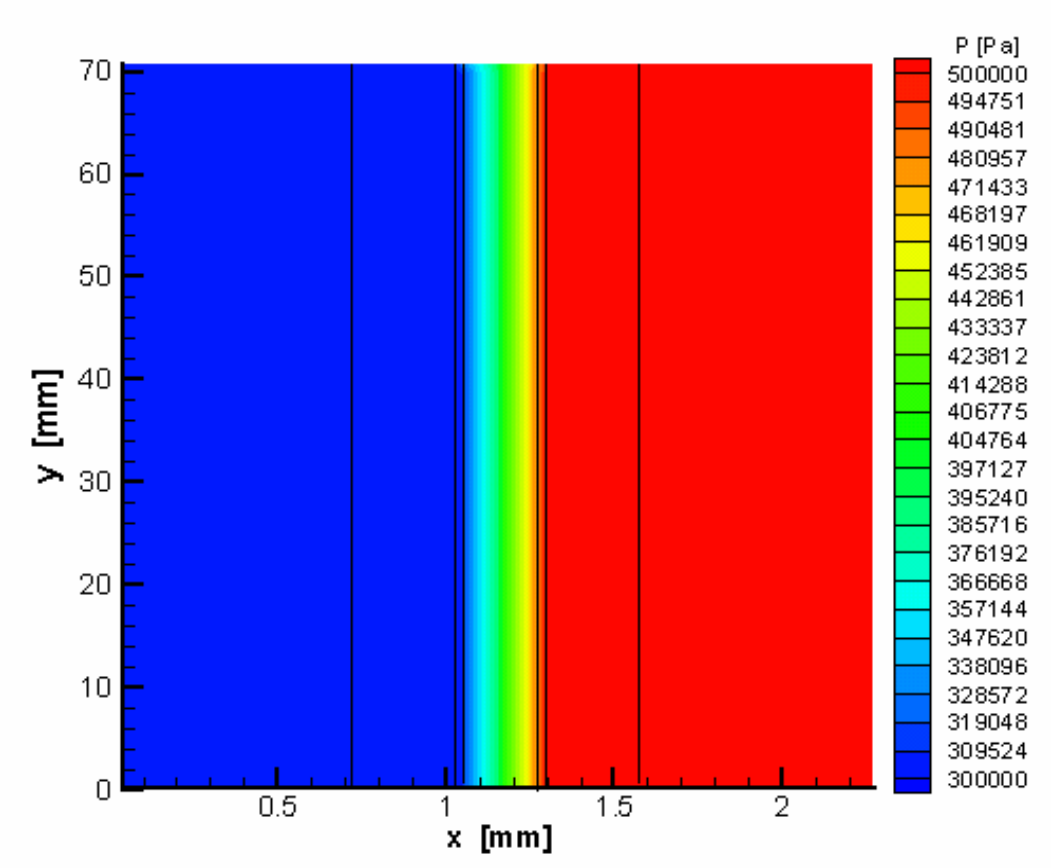

Fig.5.7 Pressure Contours throughout the cell

[Base case conditions]

5.1.4 Species Transport

The numerical solution shed light on the complex electrochemistry-flow/transport interactions in the fuel cell. Fig.5.8 below shows the oxygen mole fraction 2-D contours throughout the cell.. It is obvious that oxygen is being depleted along the gas channel as it diffuses through the porous media to the active sites at the cathode catalyst layer to be consumed by the electrochemical reaction. The membrane is assumed to be impermeable to oxygen and thus it can not penetrate it. This assumption has been dealt with numerically by assigning the source term a sufficiently large value that freezes the oxygen mass fraction to a value of zero as evident by the contours below.

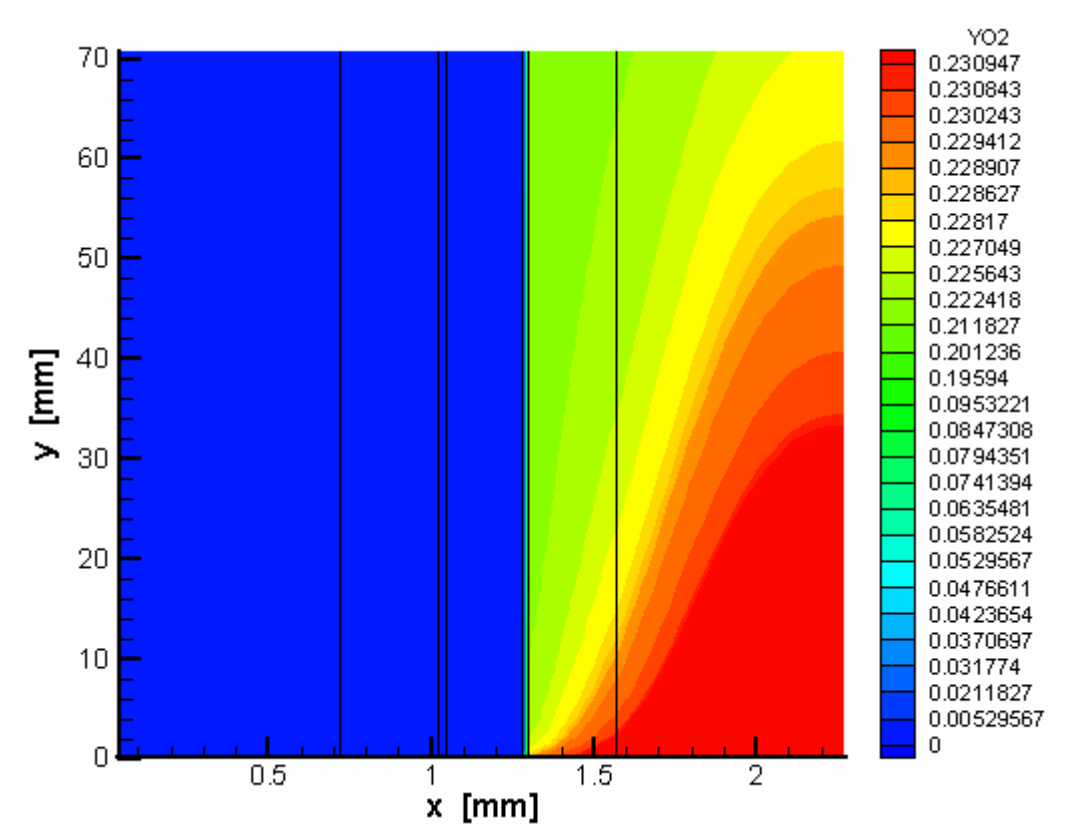

Fig 5.8 2-D contours of Oxygen mass fraction throughout the cell
[Base case condition,Vcell=0.6 volt]

In a like manner the hydrogen mass fraction 2D contours have been plotted in Fig.5.9 a similar behavior is exhibited by the hydrogen as shown where the anode stream is being progressively depleted of hydrogen along the channel since it is consumed by the electrochemical reaction, and thus the stream becomes gradually diluted along the

channel especially at high fuel utilization conditions(that are necessary for highest possible fuel efficiency) like those employed in this simulation and thus the hydrogen transport to the reaction sites becomes a limiting step for the cell current density in this case, this is referred to as the "down-the-channel" effect. This problem could be alleviated by using large flow rates at the expense of fuel utilization [7].

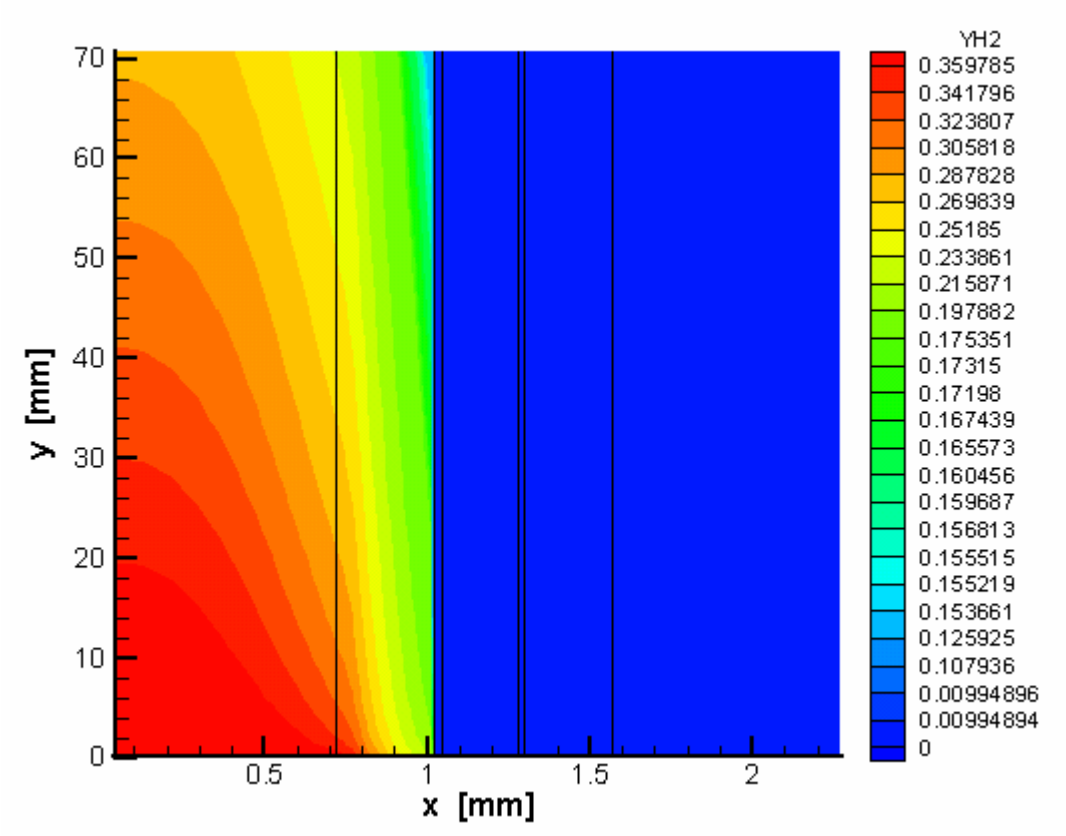

Fig 5.9 2-D contours of Hydrogen mass fraction throughout the cell
[Base case conditions, Vcell=0.6 volt, 100 % H2]

The above figure (Fig 5.9) is for the case of pure hydrogen being supplied to the cell. In cases where the anode stream is diluted with Nitrogen the 2D contours will be different, as shown in Fig.5.10 where the down the channel effect is less evident as hydrogen diffusion through the porous media is limited and thus the anode stream is not being depleted of hydrogen as much as in the case of pure hydrogen.

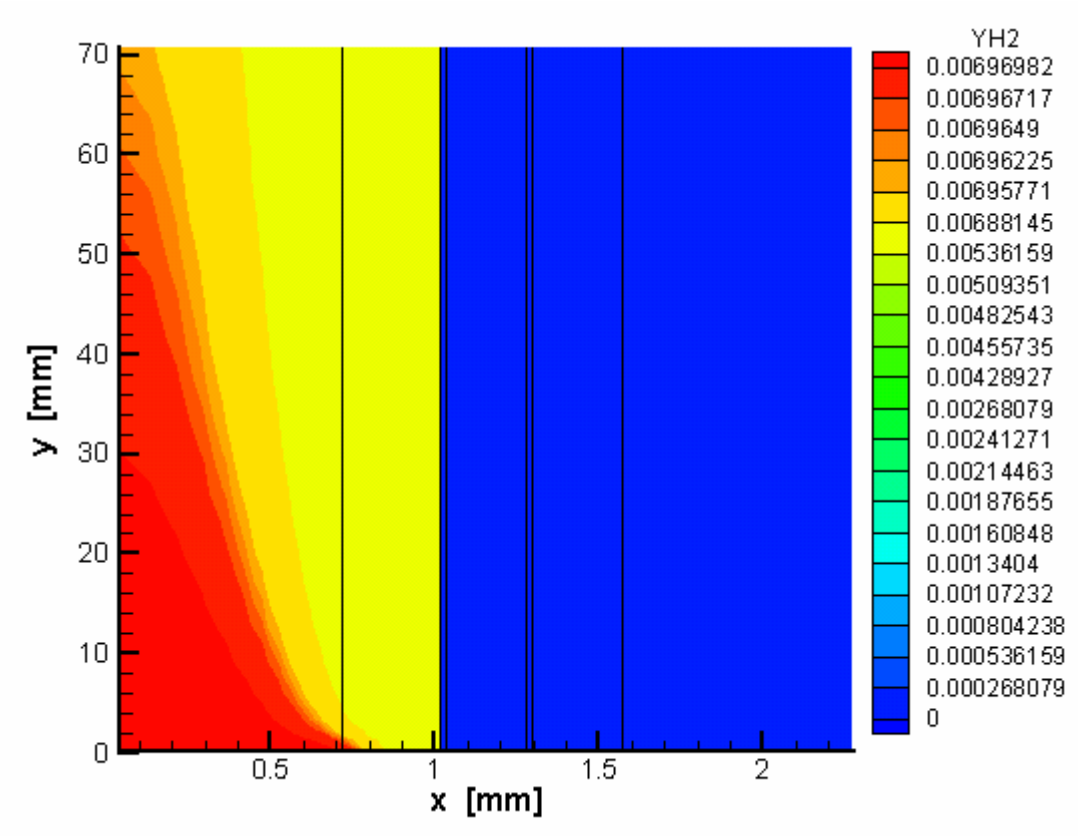

Fig 5.10 2-D contours of Hydrogen mass fraction throughout the cell
[Base case conditions, Vcell=0.6 volt, 10 % H2]

As for water vapor, the 2-D contours are shown in Fig.5.11 Where the fuel stream is assumed to be fully humidified whereas the incoming air is assumed to be dry. Water is being produced by the electrochemical reaction at the cathode catalyst layer and then diffuses to other low concentration regions of the cell. Fuel humidification is performed so that we could avoid dehydration of the membrane at the anode side (which is more likely to dry out) which leads to loss of protonic conductivity and thus increased membrane resistance. However, too much water could result in flooding of the electrodes, blocking the pores that allow reactant transport, and thus severely affecting the reaction rate. Therefore, it is necessary to balance these two phenomena. Water management is generally a critical performance issue for polymer membrane fuel cells.Fig.5.12 shows the 2-D contours of water vapor through the PEMFC where the cathode stream was assumed fully humidified and the fuel stream was assumed dry and Fig.5.13 is for the common case where the two streams are fully humidified.

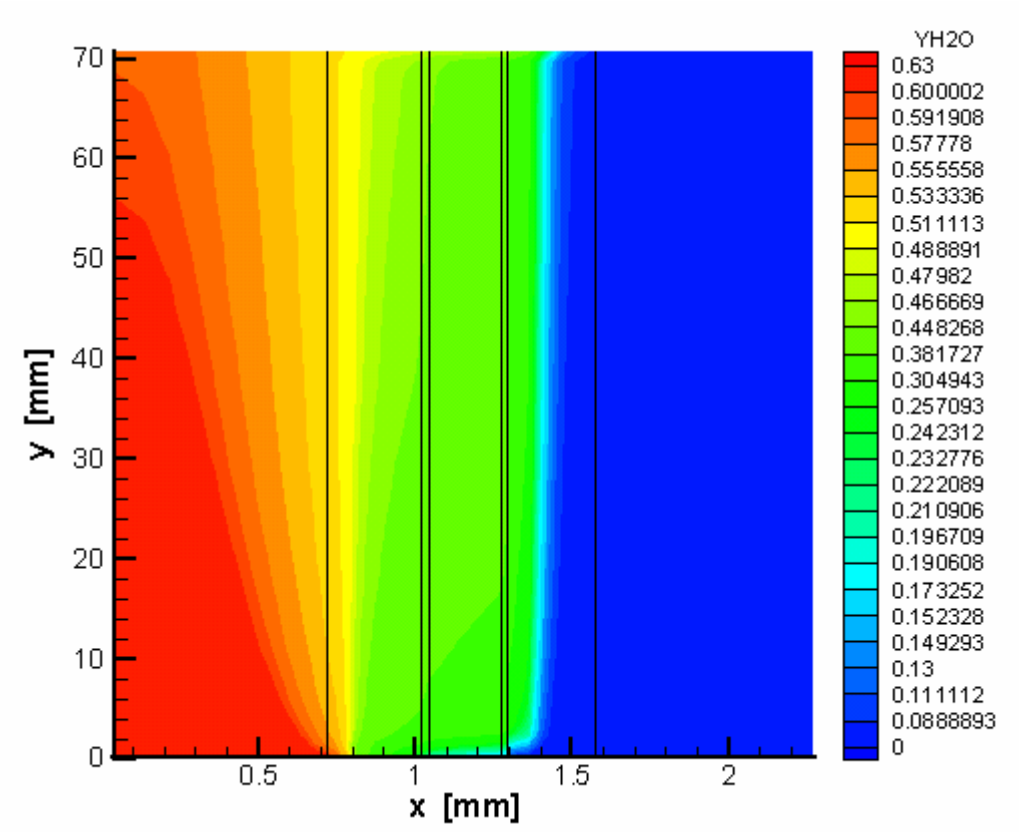

Fig 5.11 2-D contours of water vapor mass fraction throughout the cell
[Base case conditions, Vcell=0.6 volt]

Those simulations display the capabilities of the present model in accurately and thoroughly predicting the water vapor distribution throughout the cell. This model could thus be readily linked to other models to study the water management of the cell and to control the humidification processes of the feed streams.

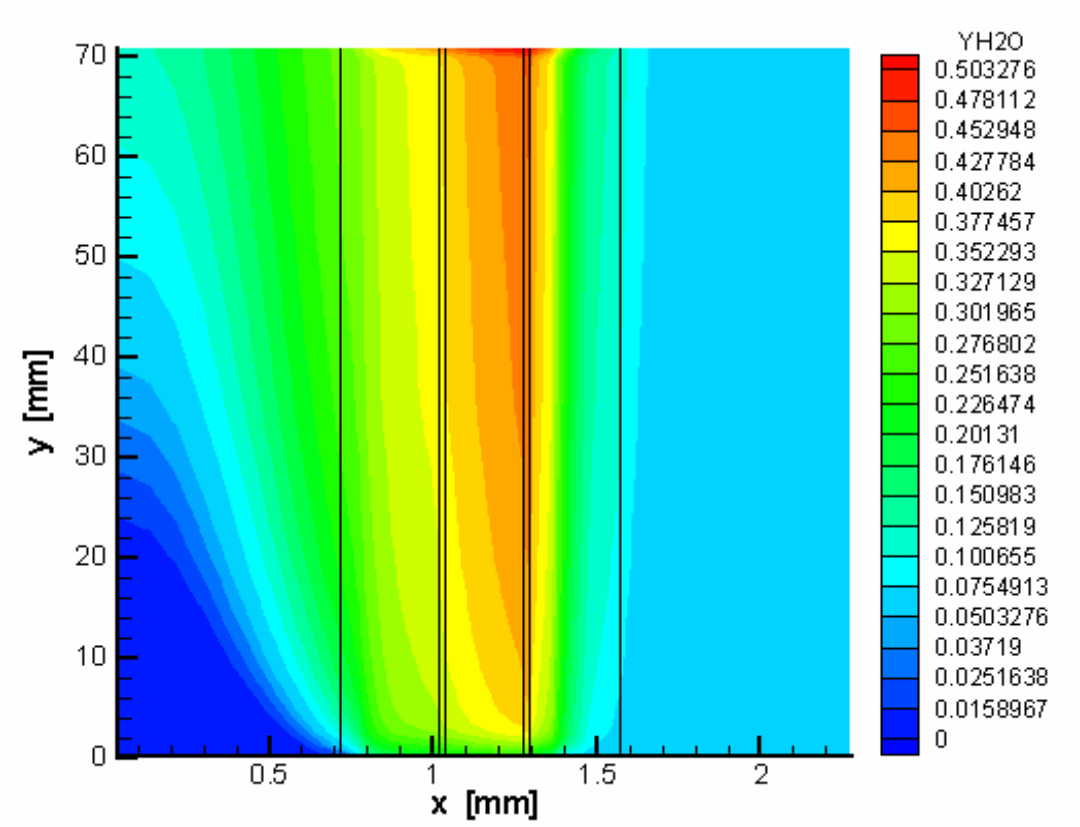

Fig 5.12 2-D contours of water vapor mass fraction throughout the cell
[Base case conditions, Vcell=0.6 volt, $X_{H2O,-}$= 0.0]

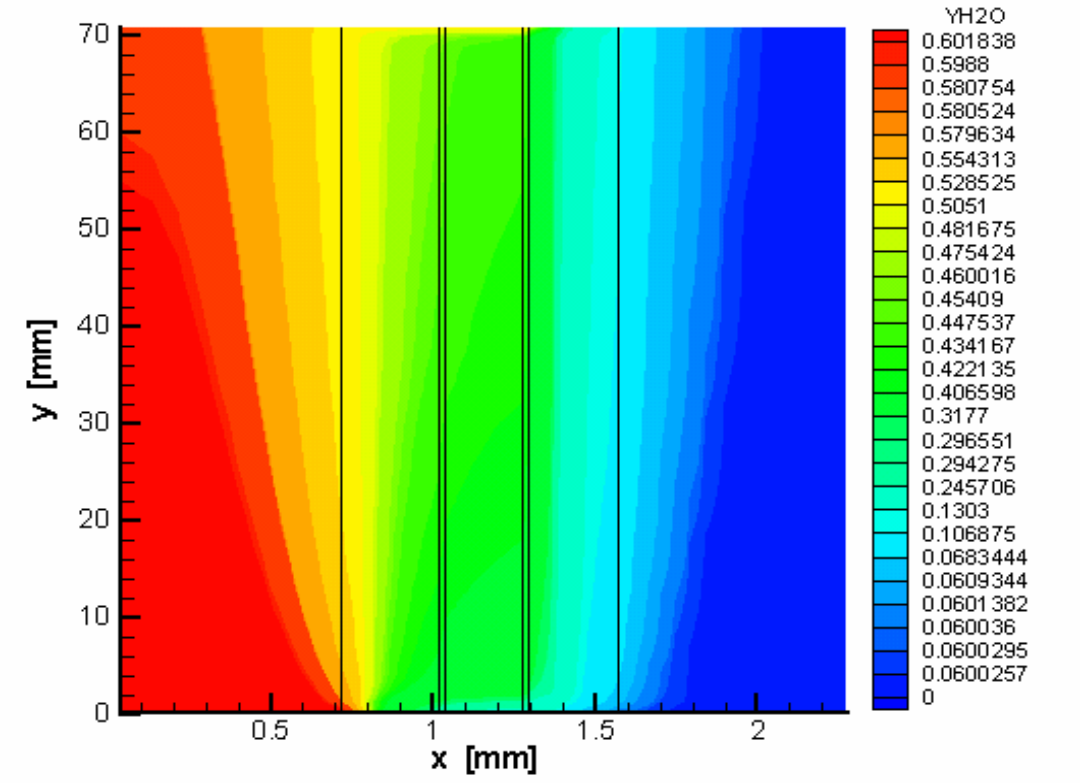

Fig 5.13 2-D contours of water vapor mass fraction throughout the cell
[Base case conditions, Vcell=0.6 volt, both streams fully humidified]

5.1.5 Current density distribution

Figure 5.14 displays the local current density distributions at various average current densities along the axial direction of fuel cell. The current density distributions are almost uniform at all cell current densities due to the small cell and high stoichiometric flow ratios employed in these experiments [7]. Fig.5.15 shows the current densities distribution obtained by [7] which is in good agreement with the results of the present model.

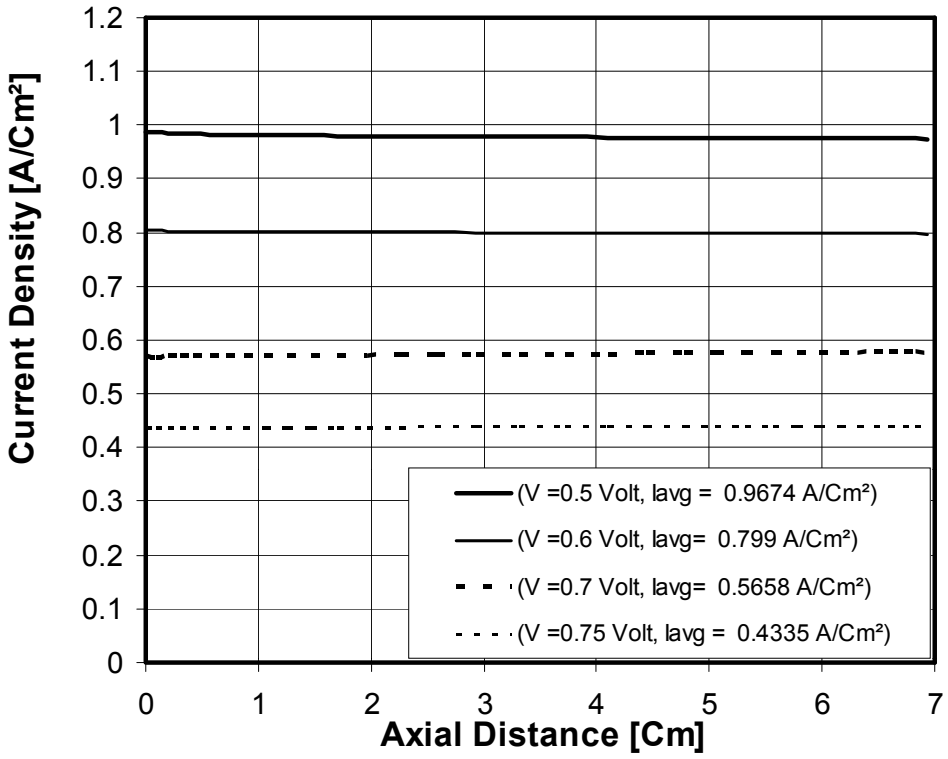

Fig.5.14 Computed Local current density distributions in the axial (y) direction

[Base case conditions]

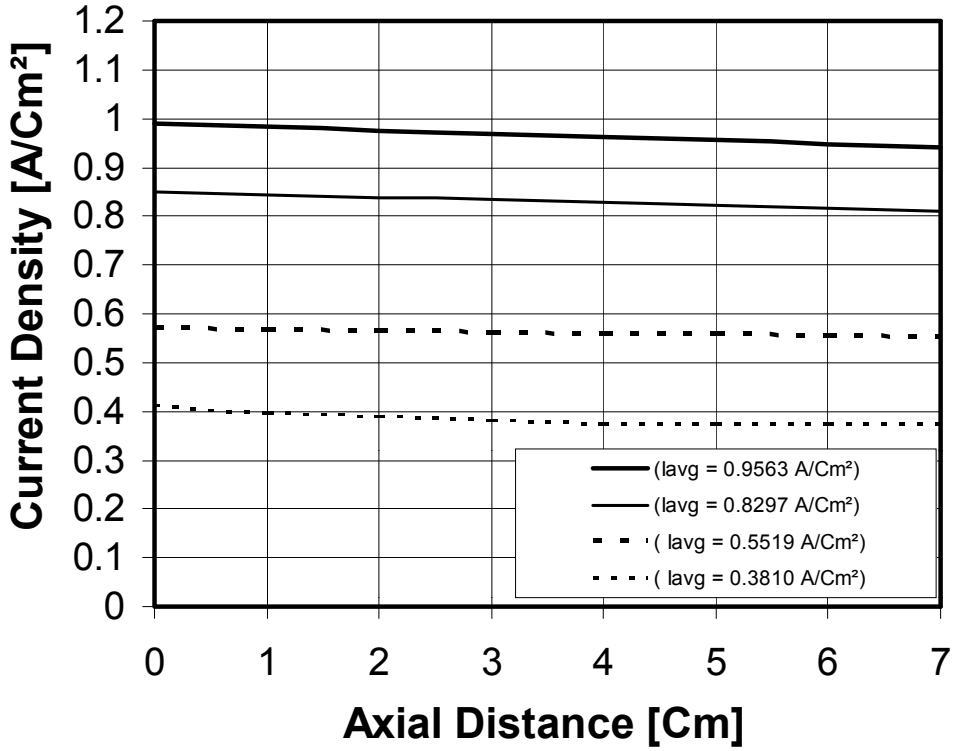

Fig.5.15 Local current density distributions in the axial (y) direction, Adapted from [7]

5.1.6 Membrane phase potential profiles

Figure 5.16 shows predicted profiles of the membrane phase potential across the anode catalyst layer, the membrane, and the cathode catalyst layer at various axial locations for *a* cell voltage of 0.6 V. The membrane phase potential is in reference to the anode solid potential of zero it is to be noted that the solution exhibited in Fig5.16 satisfies the zero flux boundary conditions imposed at the boundaries of the computational domain and thus insures that no protons would escape through the boundaries. This is most evident in Fig 5.17 Where the Membrane phase potential contours were plotted throughout the Catalyst layers / membrane combined sub-domain where Poisson's equation for the membrane phase potential was applied and solved. It is to be noted that the potential is constant throughout the gas diffuser layers.

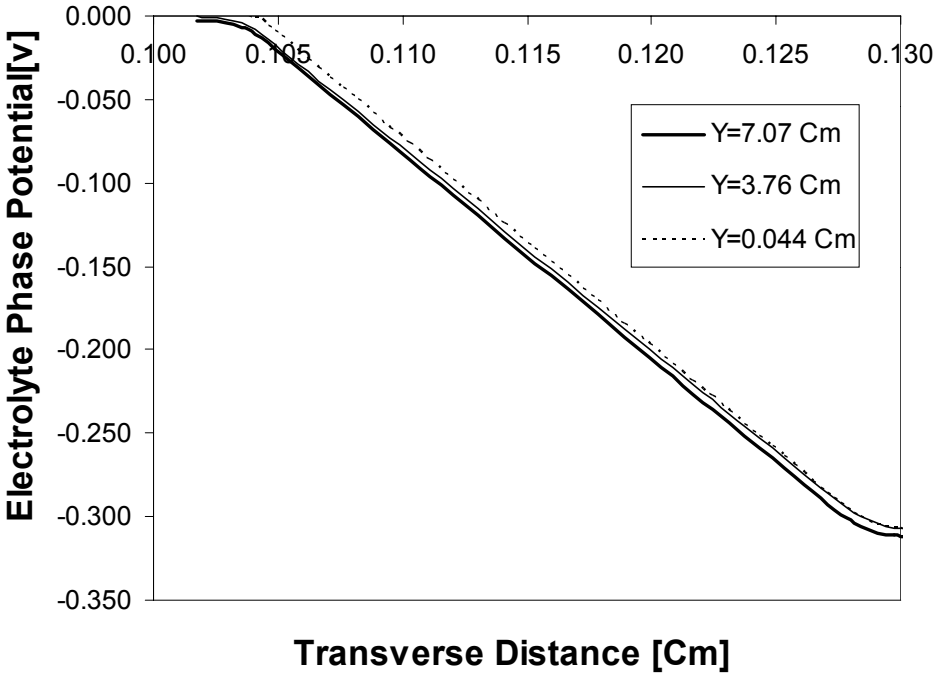

Fig.5.16 Computed phase potential distributions in the transverse (*x*) Direction [Base case conditions, Vcell = 0.6 volt]

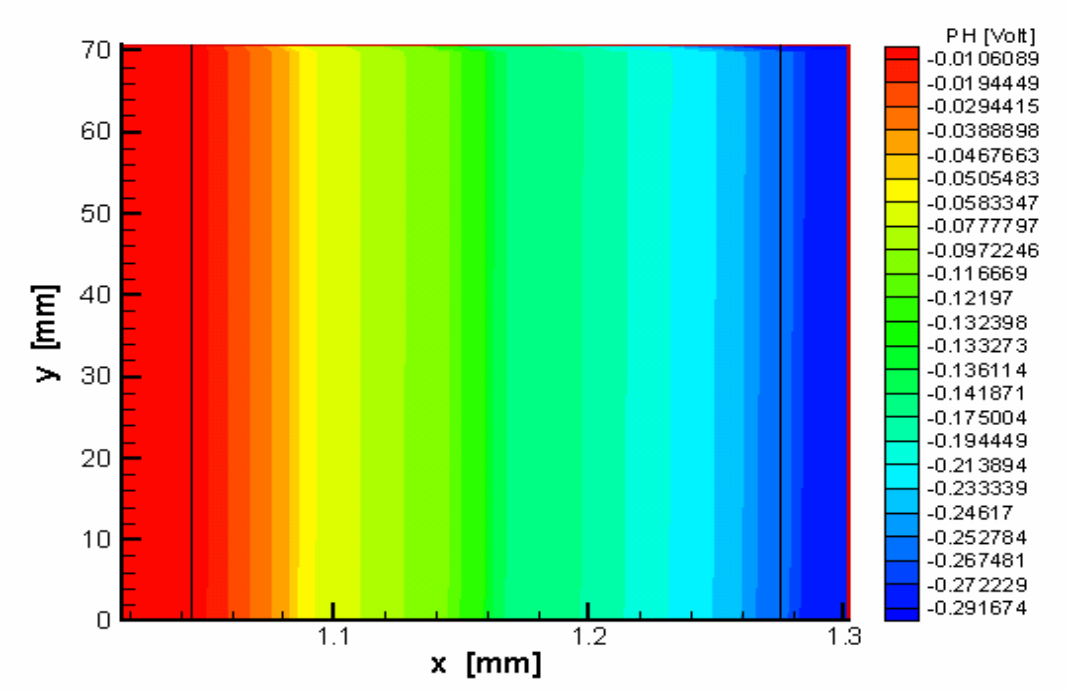

Fig.5.17 Computed phase potential contours throughout the catalyst layers / Membrane regions [Base case conditions, Vcell =0.6 volt]

A careful investigation of the contours reveals the absence of any fluxes at the domain walls which satisfies the imposed boundary conditions. Fig5.18 below displays the membrane phase potential distribution at different axial locations at a cell voltage of 0.85 V

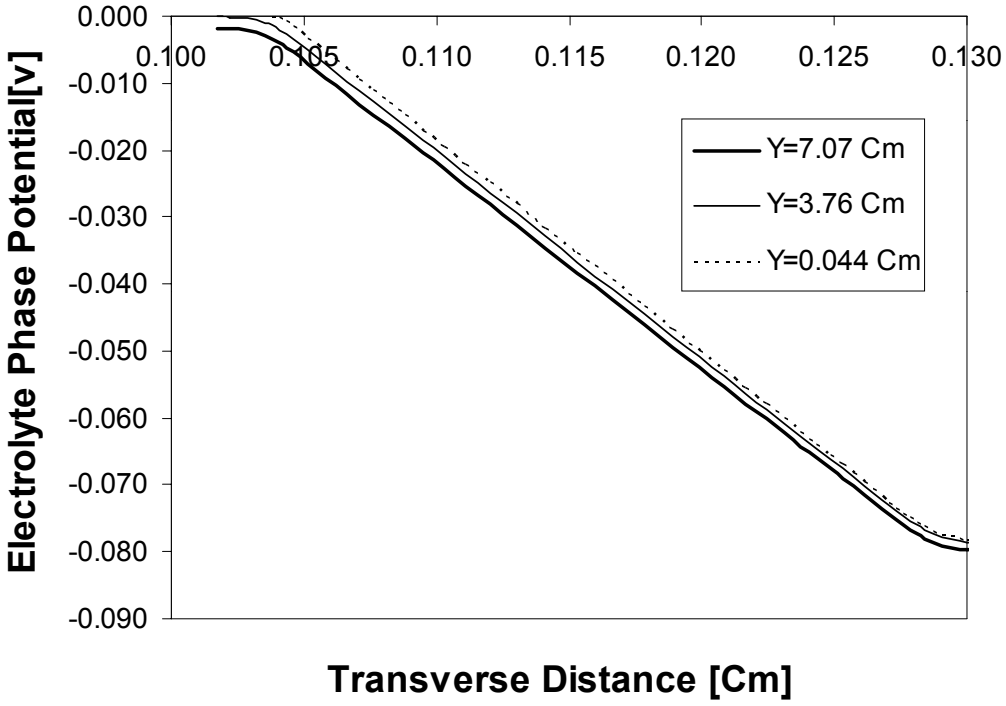

Fig.5.18 Computed phase potential distributions in the transverse (*x*) Direction [Base case conditions, Vcell = 0.85 volt]

Fig.5.19 and 5.20 display the potential phase distributions obtained by [7]. Careful examination of those curves reveals the good agreement between the two numerical solutions.

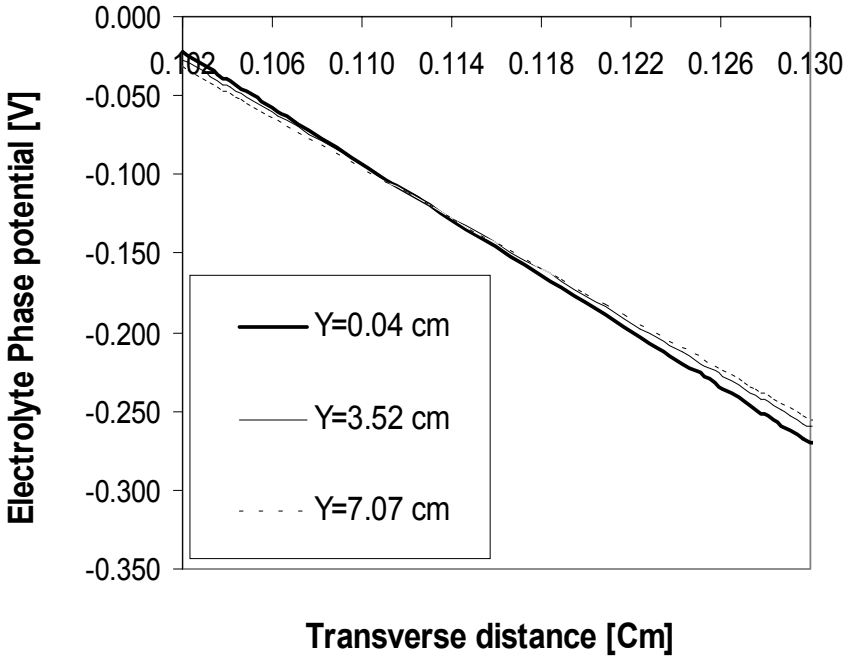

Fig.5.19 Phase potential distributions obtained by [7]
[Base case conditions, Vcell = 0.6 volt]

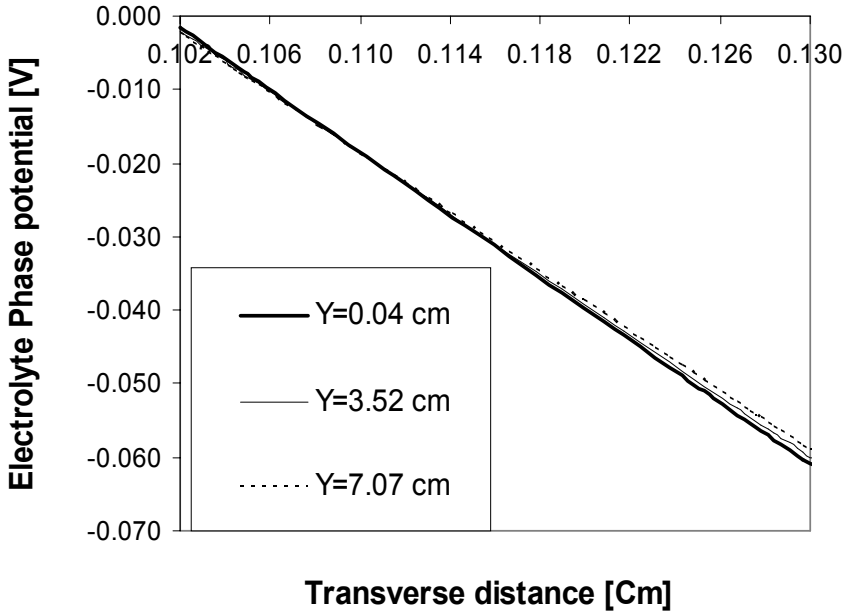

Fig.5.20 Phase potential distributions obtained by [7]
[Base case conditions, Vcell = 0.85 volt]

5.1.7 Oxygen enrichment effects

In order to alleviate mass transport losses at the cathode side, the incoming air stream is sometimes enriched with oxygen. The effect of using pure oxygen instead of air has been experimentally determined by [34]. Figure 5.21 shows the Polarization curves of a fuel cell operating at two different pressures at a temperature of 50 °C for both air and pure oxygen that were obtained by [34].

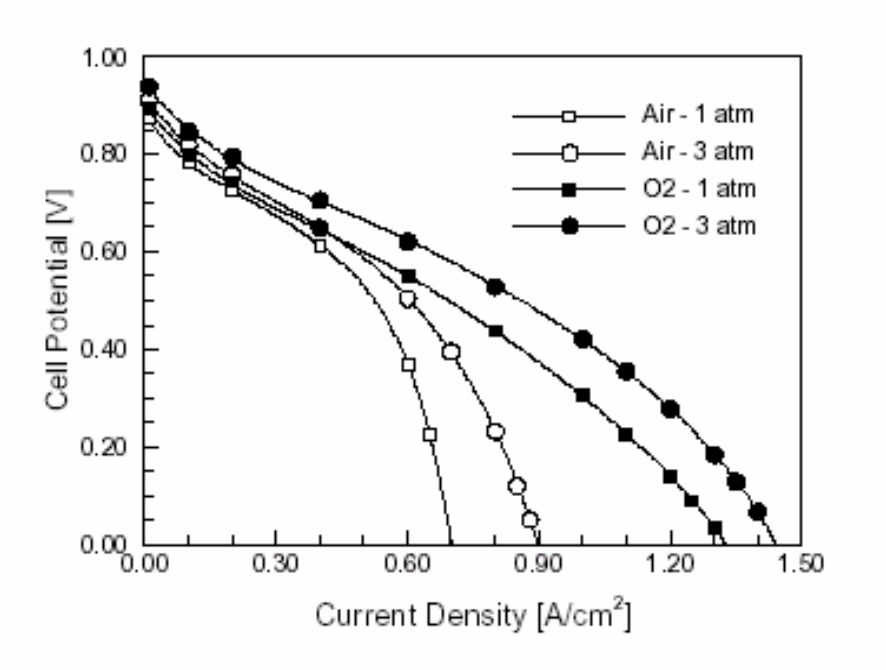

Fig.5.21 experimentally measured fuel cell performance at 50 °C for air and pure oxygen

A series of runs were made at a stoichiometric ratio of 3.0 at the cathode side and 2.4 at the anode side. The anode pressure was fixed at 3.0 bar while the cathode pressure was 5.0 bar for one simulation and 3.0 for the other and the two feed streams were assumed fully humidified. In all, the results as shown in Fig.5.22 exhibit the same trend as those displayed in fig.5.21 however, quantitative comparison can not be made since the conditions of the experiment of [34] were not fully reported.

Fig.5.23 displays the 2D contours of the oxygen mass fraction throughout the cell.

It is evident that the "down-the-channel" effect decreased and thus the concentration overpotential along the gas channel is less than the case where air is used instead of pure oxygen leading to higher cell current densities and better cell performance.

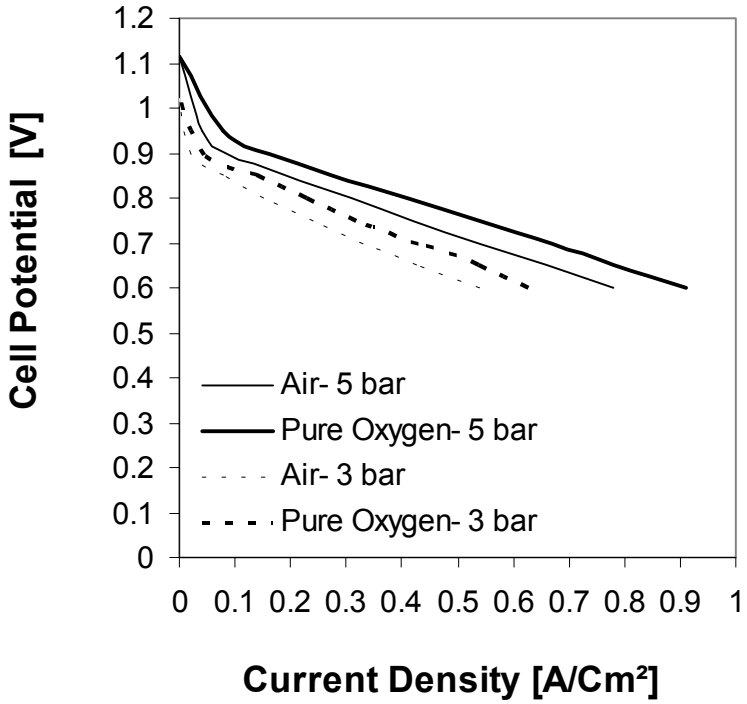

Fig.5.22 Computed polarization curves under Air

And pure oxygen operating conditions

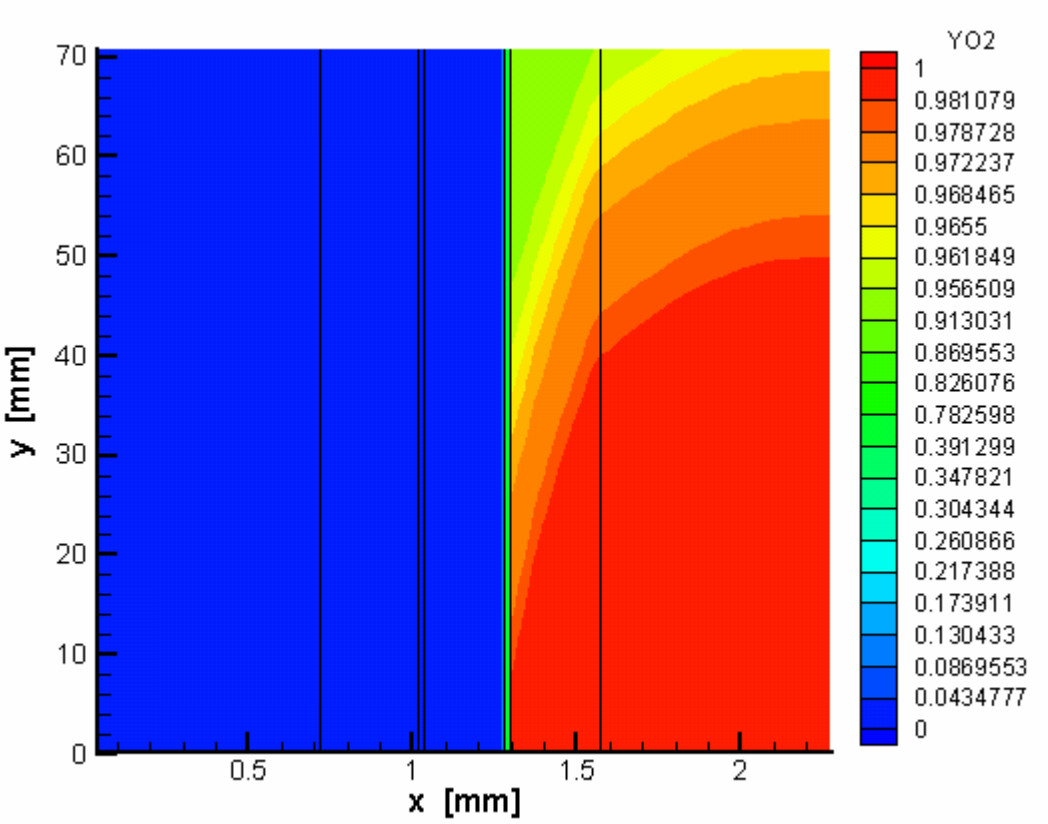

Fig.5.23 2-D contours of Oxygen mass fraction throughout the cell

[Base case conditions, Pure Oxygen supplied , V=0.6 Volt]

5.1.8 Hydrogen dilution effects

To the best of the authors' knowledge, the hydrogen dilution effect has not been thoroughly investigated experimentally except for the data found in a meeting abstract [20] accordingly; this data can not be considered a bench-mark. It is to be noted that, when reformate gas is used as the anode feed; the hydrogen mole fraction at the anode inlet is significantly lower than that in the pure hydrogen condition (*i.e.,* hydrogen plus water vapor only) This in turn, might lead to mass-transfer limited cell performance especially at high current densities where hydrogen is to be abundantly supplied to the reaction sites. A series of simulations for different hydrogen inlet fractions at the anode were carried out to illustrate this effect. In all these simulations, the stoichiometric flow ratios of fuel and oxidant are fixed at 2.4 and 3.0 at 1 A/cm², respectively. The conditions of the experiment found in [20] are not known except for the cell temperature and hydrogen stoichiometry.Fig5.24 displays the results of the experiment found in [20].

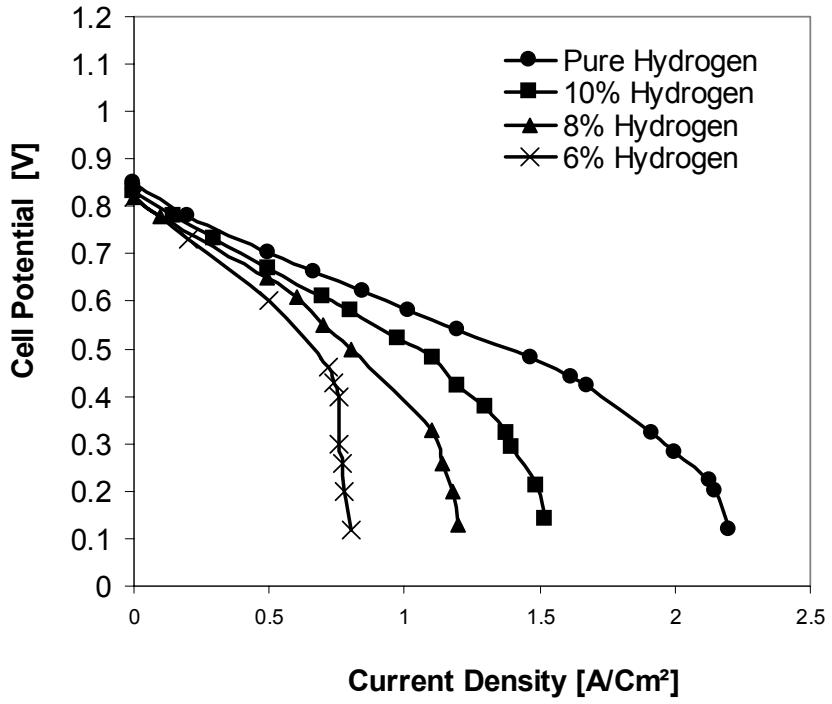

Fig.5.24. Experimentally determined polarization curves under H_2 dilution conditions, adapted from [20]. [Cell Temperature 80 °C, H_2 stoichiometry 2.4 at 1.0 A/Cm²]

It shows smooth decrease in the current density with hydrogen dilution and there is no hydrogen percentage below which the cell performance is catastrophically affected [20]. Figure 5.25 shows the computed current density under hydrogen dilution conditions. It is evident that it decreases to a somewhat big extent –but not as much as the experiment-for all the current densities, in qualitative agreement with the experiment found in [20] however quantitative comparison is not possible due to the lack of specific information about the conditions of this experiment. The reason why the effect of hydrogen dilution is not as much as in the experiment is that the present model assumes the anode kinetics to be very fast and accordingly, whatever small is the quantity of hydrogen reaching the active area of the anode catalyst layer, it is instantly consumed by the electrochemical reaction and thus hydrogen kinetics is not the rate-limiting step for the cell performance. In all, further more detailed study of the hydrogen dilution effect is required both experimentally and theoretically to determine the factors affecting this phenomenon and to accurately quantify its impact on the cell performance. The present model takes into account the anode kinetics through Eq.3.8 representing all the cell conditions including operation under hydrogen dilution and low current density conditions which might not be true and is to be scrutinized through those studies. At low current densities the consumption rate of the hydrogen available at the reaction sites may not be high leading to saturation of the catalyst surface with hydrogen and consequent zero order kinetics in which the rate of the electrochemical Reaction would only depend on the electrode potential, temperature and the active area of the catalyst and thus mass transfer limitations would not impact the cell performance. On the contrary, at high current densities the catalyst surface is being completely depleted of hydrogen and this might lead to very high concentration overpotentials had the supply of hydrogen been inadequate. Those behaviors are nonetheless not shown by the experiment in [20] which again, could not be considered as a benchmark. It is to be noted also that the present experiment separates the fuel utilization issue from the hydrogen dilution issue through the use of high stoichiometric flow ratios leading to high fuel utilization conditions (which are rarely achieved in practice) On the contrary, low fuel utilization reduces the down-the-channel effect and thus could possibly well interact with the hydrogen dilution to

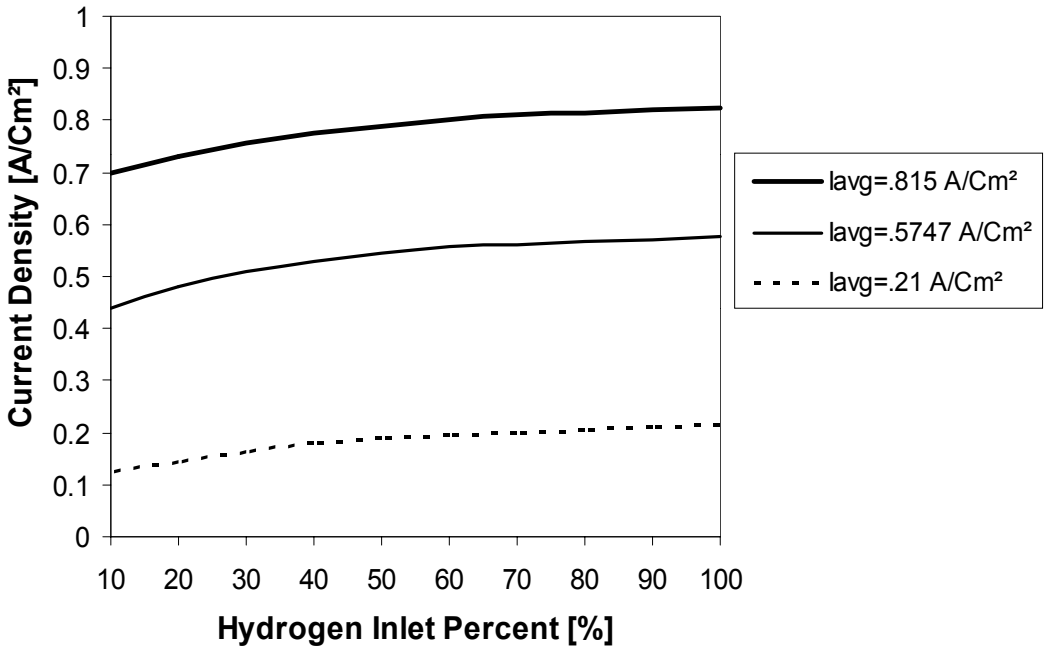

Fig.5.25 Computed current densities under H_2 dilution conditions
[Base case conditions, H_2 stoichiometry 2.4 at 1.0 A/Cm²]

Impact the cell performance, which is accordingly to be further investigated.

5.1.9 Onset of Two-phase Flow

In the present model, it is assumed that water only exists in the vapor state. However, if the electrochemical reaction rate is sufficiently high, the water produced is apt to condense into the liquid phase. In this situation, two-phase flow and transport may have to be considered. Figure 5.26 displays water vapor mole fraction profiles along the interface between the catalyst layer and gas diffuser on the cathode side where there is the highest content of water vapor. When the cell current density is higher than about 0.6 A/cm^2 (the same value predicted by [7]), the water vapor mole fraction along the catalyst layer/gas diffuser interface already exceeds the saturated level, *i.e.,* $X_{H2O}^{sat} = 0.093541$ at a pressure of 5 atm and a cell temperature of 353 K. Hence, it suggests that the two-phase flow regime starts at intermediate current densities and thus the present model is capable of predicting the cell performance up to about 0.6

A/cm^2. Nonetheless, a single-phase analysis such as the present model and many existing models [7, 10, 11, 13, 35, 36, and 37] still provides a good first approximation of cell performance for current densities above 0.6 A/cm^2. This is true because the water distribution affects the electrochemical process and oxygen transport in the air cathode primarily in two ways. First, the presence of liquid water affects the water content in the membrane and thus slightly alters its ionic conductivity. More important, liquid water present in the gas diffusion cathode hampers oxygen transport to the catalyst layer [7]. However, recent two-phase calculations[40, 41] indicated that a small amount of water is present in the cell up to a current density of about 1.5 A/cm^{2}and thus these effects are likely to be minimal[7].

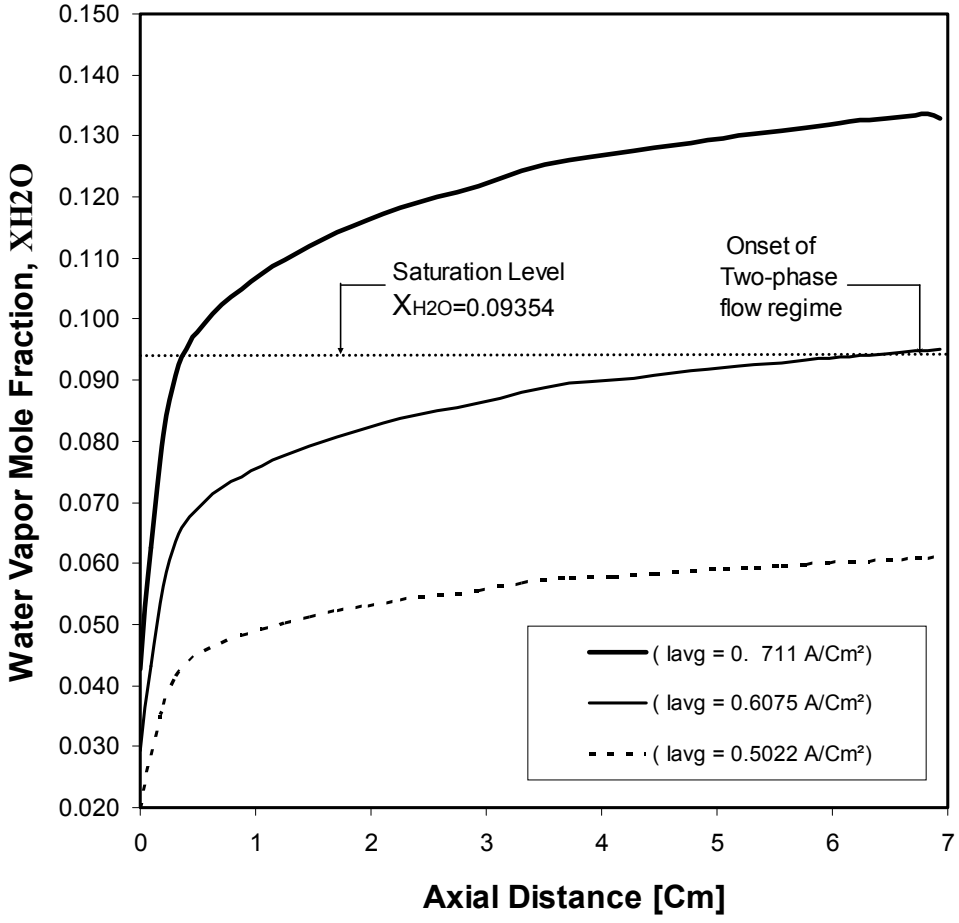

Fig 5.26 Computed water vapor mole fraction along the cathode GDL/CL interface

Fig5.27 Below displays the water vapor mole fraction profiles obtained by Um et al. It readily shows that the onset of two-phase flow occurs at a current density of about 0.6 A/cm^2 which is close to the value predicted by the present solution.

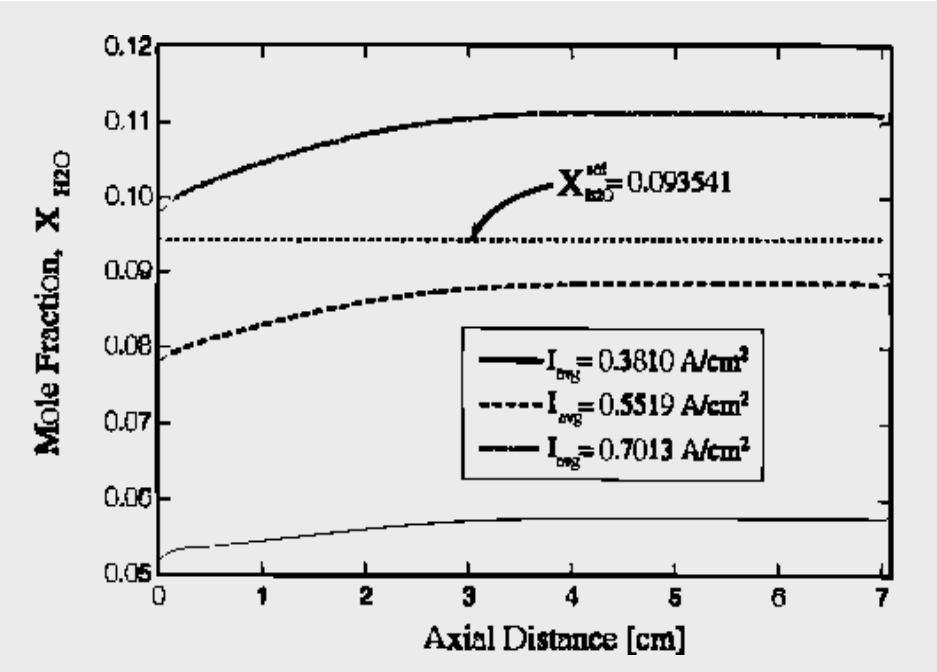

Fig5.27 Water vapor mole fraction profiles obtained by [7]

[Base case conditions]

Chapter Six

CONCLUSIONS AND SUGGESTIONS FOR FUTURE WORK

6.1 Introduction

The present thesis work aims at developing a mathematical model that describes the complex physical phenomena occurring inside the polymer membrane fuel cells, to develop the CFD tool to solve the proposed model and to study the effect of the various operating parameters on the performance of the cell. The numerical solution obtained shed light on the interaction of the flow/transport and electrochemistry of the PEMFC and lead to more in-depth understanding of the interrelations of the different cell parameters. The CFD code has been validated against existing experimental work as well as other existing numerical solutions, even though complete similarity of the conditions of the experiments or even of the simulation parameters used in other numerical solutions could not be attained, the results of the present numerical solution agreed qualitatively with all of the existing experimental work and numerical solutions. Few suggestions come to mind for building up on the existing thesis work towards more in-depth understanding of the physics of the PEFMC and more elaborate quantification of the performance of the cell under different operating conditions. Those suggestions will be discussed in the next few subsections.

6.2 Conclusions of the Present Work

The present model is capable of predicting the performance of the cell to high accuracy under the different operating conditions. A thorough examination of the results of chapter 5 leads to the following conclusions:

- Increasing the operating temperature leads to improved cell performance because of the reduced cell internal resistance, reduced activation overpotential, and overall improvement in the mass transport to the reaction sites. However the maximum possible operating temperature is limited by the maximum temperature that the membrane material can withstand without

being damaged and dehydration of the membrane which leads to its loss of the protonic conductivity and thus increased cell resistance and consequent poor cell performance.

- Increasing the cell pressure improves the cell performance up to a certain limit beyond which any further pressurizing can not be justified.
- Controlled humidification of the feed streams is desirable to alleviate the problem of membrane dehydration and consequent loss of protonic conductivity but it must be rigorously assessed so as to avoid flooding of the electrodes in which the pores are plugged with water which drastically hampers the transport of further reactants to the reaction sites and accordingly leads to drastic drop in the cell performance.
- Use of pure oxygen enhances the cell performance by reducing the concentration overpotential resulting from the limited transport of oxygen to the active reaction sites at the cathode catalyst layer.
- In a like manner, increasing the percentage of hydrogen in the reformate alleviates mass transport limitations on the anode side and thus leading to improved cell performance.
- The model is capable of predicting the cell performance within a relatively broad span of the cell operating voltages beyond which the two-phase flow regime starts and more elaborate mathematical model is then required to describe the cell physical phenomena.

6.3 Recommendations for Future Work,

The aim of the following recommendations is to improve the model presented in this thesis work so as to gain a more thorough understanding of the physics underlying the operation of the polymer membrane fuel cells.

- Modifying the model to take into account transient effects, in this thesis work we solved a steady-state model and thus our model is not capable of prediction of the fuel cell response to varying load conditions.
- Modifying the model to take into account the two-phase flow phenomenon occurring inside the cell.

- More elaborate determination of the different simulation parameters including electrochemistry parameters like the cathodic exchange current density and its variation with the cell operating conditions and the diffusivity of the different mixture components especially that of the water vapor throughout the membrane (In this thesis work the effect of membrane water content has been ignored and Also the membrane protonic conductivity was assumed to vary only with the temperature whereas it is known to vary with the membrane water content as well).
- More accurate determination of the open circuit voltage. Due to losses resulting from undesired species crossover from one electrode through the electrolyte and internal currents, the actual open circuit voltage is below the theoretical value (use has been made of the Nernst equation in this thesis work for the majority of the simulations).besides, the experiment had shown that it increases with the temperature on the contrary to the predictions of Nernst equation however the experimental correlation (that was employed for the effect-of-temperature simulation) does not reflect the effect of the change of the operating pressures on the open circuit voltage.
- Studying the different types of flow field design (serpentine, parallel flow, interdigitated …etc) and its effect on the cell performance regarding pressure drop and uniformity of reactants at the gas channel/porous media interface. Such a simulation would involve more detailed three-dimensional model of the fuel cell.
- Conducting a water management study which will ultimately lead to determination of the required humidification levels for the different feed streams and avoidance of the conditions leading to membrane dehydration.
- Conducting a heat management study to determine the heat generated within the fuel cell resulting from ohmic heating, phase change…etc and the heat dissipation to the coolant, cell body...etc so that we can avoid the conditions leading to high cell temperatures which might lead to damage of the polymeric membrane. Such a study would involve modifying the model by solving the energy equation (in this thesis work the temperature was assumed constant.) and incorporating the different sources of heat generation and dissipation into the energy equation and then to solve for the temperature.

- More elaborate study of the anode stream dilution effect including of course the CO poisoning effect. Such a study would require an in-depth understanding of the anode kinetics where CO is present in the anode stream, and might lead to enhancement of the cell tolerance levels to CO.

REFERENCES

1. US-DOE, Office of Fossil Energy, FETC, “Fuel Cell Handbook”, Morgantown, WV, 2000.
2. von Spakovsky M.R., Nelson D.J, and Ellis M.W. ME 5984, "Fuel Cell Systems", Class Notes, Virginia Polytechnic and State University, Blacksburg, VA, Spring 2000.
3. Hamann, C., Hamnett, A., and Vielstich, W., "Electrochemistry", Wiley-VCH, New York, New York, 1998.
4. Yammoto, O., Solid Oxide Fuel Cells, "Fundamental Aspects and Prospects", Eletcrochemica Acta, Vol.45, 2000, pp. 2423-2435.
5. Mench, M.M., Wang, C.Y., and Thynell, S.T., "An Introduction to Fuel Cells and Related Transport Phenomena", Accepted for publication in Journal of Transport Phenomena, 2001.
6. Bard, A.J., and Faulkner, L.R., "Electrochemical Methods", John Wiley and Sons, New York, New York, 1980, pp.101.
7. Um, S., Wang, C.Y., and Chen, K.S.,"Computational Fluid Dynamics Modeling Of Proton Exchange Membrane Fuel Cells",J Electrochem.Soc., Vol.147, No.12, 2000, pp. 4485
8. Sherif, S.A., Barbir, F., and Veziroglu, T.N., "Hydrogen Energy System: Fundamentals and Applications." Asia Pacific Tech Monitor, January/February 1999.
9. Olsommer B., "Mathematical Model for a PEM Fuel Cell", Internal Document, Energy Management Institute, Mechanical Engineering, Virginia Polytechnic and State University, Blacksburg, VA, 2000.
10. Springer, T.E., Zawodzinski, T.A., and Gottesfeld , S., "Polymer Electrolyte Fuel Cell Model", Journal of the Electrochemical Society, Vol. 138, No. 8, 1991, pp. 2334-2342,(a).
11. Bernardi, D.M.,and Verbrugge, M.W., , "A Mathematical Model of the Solid-Polymer-Electrolyte Fuel Cell", Journal of the Electrochemical Society, Vol. 139, No. 9,1992, pp. 2477-2491.

12. Weisbrod, K.R., Vanderborgh, N.E., and Grot S.A., "Modeling of Gaseous Flows within Proton Exchange Membrane Fuel Cells" , Proceedings 1996 Fuel Cell Seminar, Orlando, FL, 1996, pp. 635-638.
13. Gurau, V., Kakac, S., and Liu, H., "Mathematical Model for Proton Exchange Membrane Fuel Cells", AES Vol. 38, Proc. of the ASME Advanced Energy Systems Division, 1998, pp. 205-214,ASME.
14. Eikerling, M., Kharkats, YuI., Kornyshev, A.A., and Volfkovich, YuM., "Phenomenological theory of electro-osmotic effect and water management in polymer electrolyte proton-conducting membranes", Journal of the Electrochemical Society, Vol. 145 No. 8, 1998, pp. 2684-2699.
15. Yi, J.S., Nguyen, T.V., "Multicomponent Transport in Porous Electrodes of Proton Exchange Membrane Fuel Cells Using Interdigitated Gas Distributors", Journal of the Electrochemical Society, Vol. 146, No. 1, 1999, pp. 38-45.
16. Eaton, B.M.,"One Dimensional, Transient Model of Heat, Mass, and Charge Transfer in a Proton Exchange Membrane", MSC Thesis, Mechanical Engineering, Virginia Polytechnic and State University, Blacksburg, 2001, VA.
17. Genevey, D.B.,"Transient Model of Heat, Mass, and Charge Transfer as well as Electrochemistry in the Cathode Catalyst Layer of a PEMFC", MSC Thesis, Mechanical Engineering, Virginia Polytechnic and State University, Blacksburg, 2001, VA.
18. Pasaogullari, U., Wang, C.Y., "Computational Fluid Dynamics Modeling of Proton Exchange Membrane Fuel Cells Using Fluent®", Fluent User Group Meeting, Manchester, 2002, NH.
19. Berning, T., Djilali, N.,"Three-dimensional computational analysis of transport phenomena in a PEM fuel cell—a parametric study", Journal of Power sources, Vol.124, 2003, pp. 440–452.
20. Rockward, T., Zawodzinski, T., Bauman, J., Uribe, F., Valerio, J., Springer, T., and Gotteesfeld, S., " The performance of polymer electrolyte membrane fuel cells operating on diluted hydrogen", The Electrochemical Society Meeting Abstracts, Vol. 99-1, Seattle, May 2-6, 1999, WA.

21. Hong, J.K.,Zook, L.A., Inbody, M.,Tafoya, J., and Vanderborgh, N.E., Abstract 570, The Electrochemical Society Meeting Abstracts, Vol. 99-1, Seattle, May 2-6, 1999,WA.
22. Meng, H., Wang, C.Y.,"Electron Transport in PEFCs" , Journal of the Electrochemical Society, Vol. 151 (3), 2004, A358-A367.
23. Berning, T.,"Three-Dimensional Computational Analysis of Transport Phenomena in a PEM Fuel Cell", Ph.D. Thesis, Department of Mechanical Engineering, University of Victoria, 2002.
24. Parthasarathy, A., Srinivasan, S., and Appleby, J., J. Electrochem Soc., Vol.139, 1992, pp.2530.
25. Bird, R.B., Stewart, W.E., and Lightfoot, E.N., "Transport Phenomena", John Wiley & Sons, New York, 1960.
26. Kumar, A. , and Reddy, R,G.,"Modeling of Polymer Electrolyte Membrane Fuel Cell with Metal Foam in the Flow Field of the Bipolar/End Plate",J.Power Sources, 114,2003,pp.56,62.
27. Ticianelli, E.A., Derouin, C.R., and Srinivasan, S., J. Electroanal. Chem., 1988, pp.251, 275.
28. Bernardi, D.M., and Verbrugge, M.W., AIChE J., 37, 1991, pp.1151.
29. Fluent Inc, "Fluent 6.0 User's Manual ", Centerra Resource Park, Lebanon, 2000, NH.
30. Versteeg, H.K., and Malalasekera, W., "An Introduction to Computational Fluid Dynamics", Addison Wesley Longman, London (1995).
31. Huang, P.G., and Leschziner, M.A., "An Introduction and Guide to the Code"TEAM", University of Manchester, 1984.
32. Gustavo, G., and Jen, T.C., "Numerical Analysis of the Hydrodynamics of the Flow in an Axially Rotating Heat Pipe", Internal report, Department of Mechanical Engineering, University of Wisconsin, Milwaukee, Milwaukee, 2001, WT53211.
33. Patankar, S.V.,"Numerical Heat Transfer and Fluid Flow", Hemisphere Publishing Corporation, USA, 1980.
34. Kim, J., Lee, S.M., Srinivasan, S., and Chamberlin, C.E., "Modeling of proton exchange membrane fuel cell performance with an empirical equation", J. Electrochem. Soc. 142 (8) ,1995, pp. 2670–267.

35. Beavers, G.S., Sparrow, E.M., and Mangnuson, R.A.,"Experiments on Coupled Parallel Flows in a Channel and a Bounding Porous Medium", Trans. ASME, J. Basic Eng.,Vol. 30, 1970, pp.843.
36. Dagan, G., "Flow and Transport in Porous Formations", Springer-Verlag, Berlin , 1989.
37. Springer, T.E., Wilson, M.S., and Gottesfeld, S., Journal of the Electrochemical Society, Vol. 140, 1993, pp. 3513.
38. Fuller, T.F., and Newman, J., J. Electrochem.soc., Vol.140, 1993, pp.1218.
39. Nguyen, T.V., and White, R.E., J. Electrochem.soc., Vol.140, 1993, pp.2178
40. Wang, C.Y., Wang, Z.H., and Pan, Y., Proceedings of ASME Heat Transfer Division, HTD-Vol, 364-1, ASME, New York, 1999, P.351.
41. Nguyen, T.V.,"Tutorials in Electrochemical-Engineering Mathematical Modeling", R. F. Savinell, J. M. Fenton, A. West, S. L. Scanlon, J. Weidner, Editors, PV 99-14, p. 222, The Electrochemical Society Proceedings Series , Pennington, NJ, 1999.

APPENDICES

APPENDIX A

Flow Chart of the Original TEAM Code

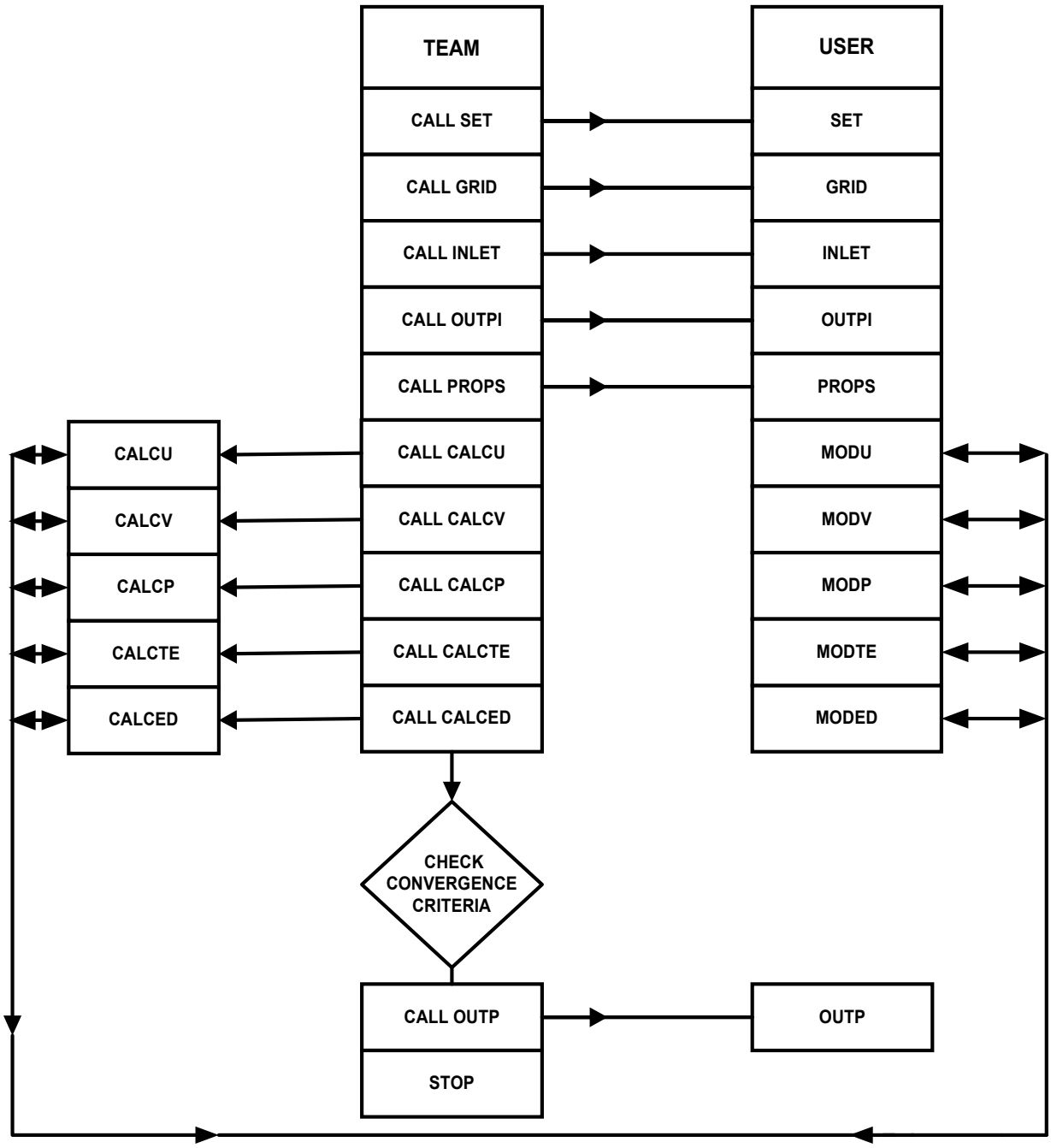

APPENDIX B

Flow Chart of the VTC Numerical Algorithm

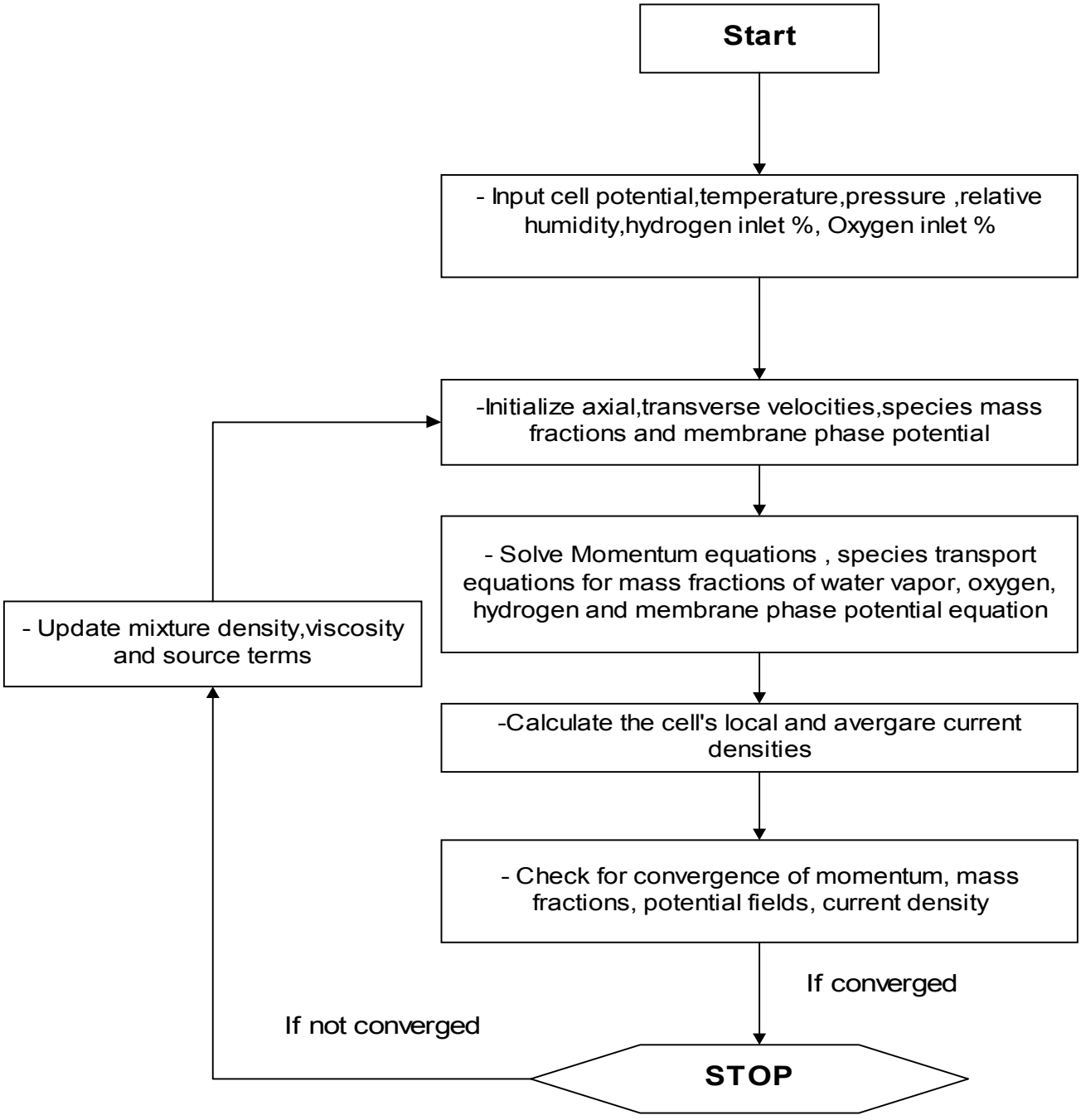

APPENDIX C

Flow Chart of the PEMCU Code

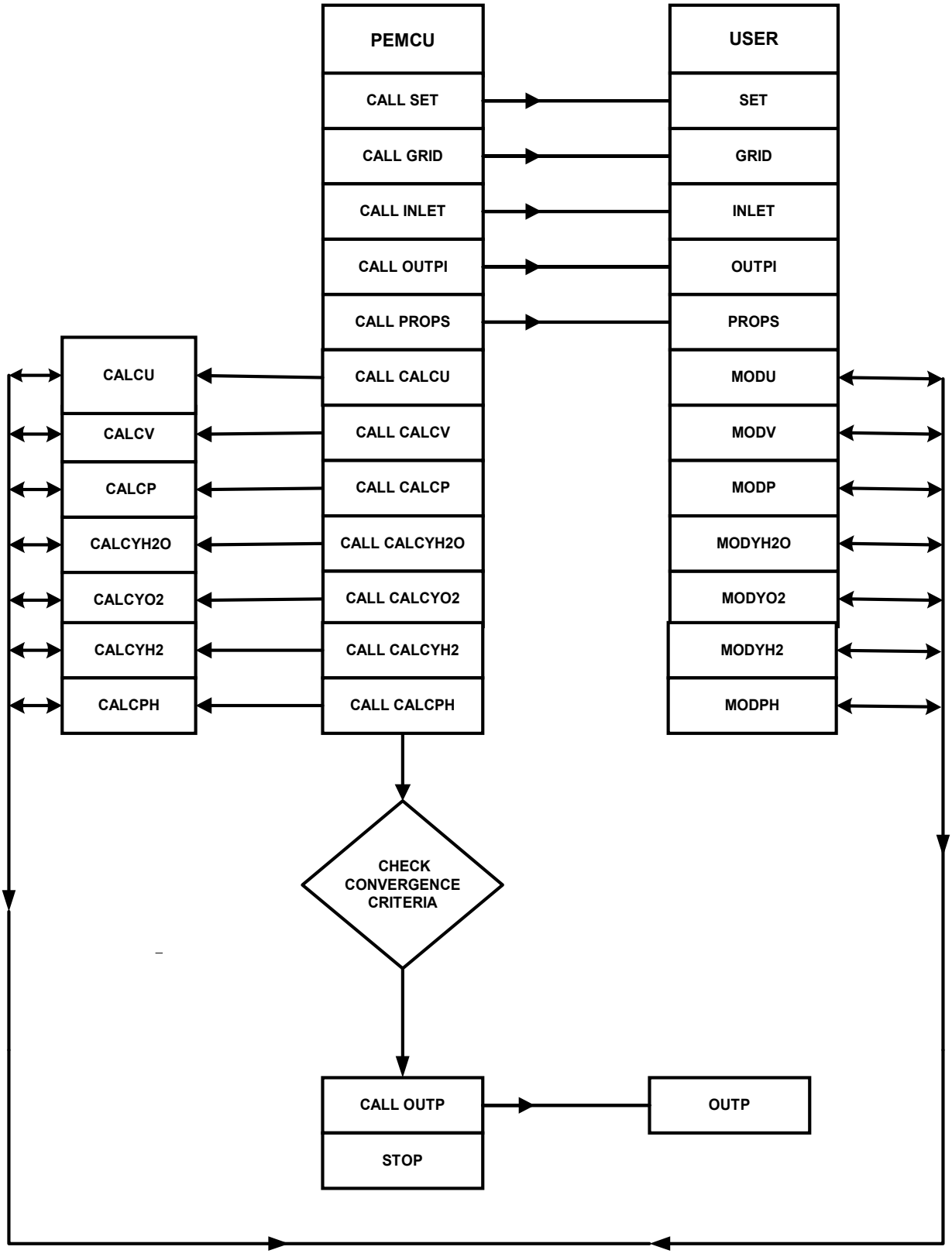

APPENDIX D

Base Case Parameters

Physical Quantity	Value*
Cathode pressure	5 bar
Anode pressure	3 bar
Air stoichiometric flow ratio ζ_+	3.
Fuel stoichiometric flow ratio ζ_+	2.8
Cell temperature	80 °C
Relative humidity of inlet air	0.0 %
Relative humidity of inlet fuel	100%
Reference exchange current density × area of anode, aJ_a^{ref}	1.4E11 A/m^3
Reference exchange current density × area of cathode, aJ_c^{ref}	6000. A/m^3
Oxygen diffusivity in gas	5.2197E-06 m^2/s
Hydrogen diffusivity in gas	2.63E-06 m^2/s
Water vapor diffusivity at the anode side	0.733E-6 m^2/s
Water vapor diffusivity at the cathode side	0.49E-06 m^2/s
Dissolved oxygen diffusivity in active layer and membrane	2.0E-8 m^2/s
Dissolved hydrogen diffusivity in active layer and membrane	2.59E-10 m^2/s
Hydraulic permeability of membrane, kp	1.8E-18 m^2
Permeability of backing layer, K	1.76E-11 m^2
Electrokinetic permeability, k_Φ	7.18E-20 m^2
Fixed site charge, Z_f	-1
Anodic transfer coefficient,α_a	2
Cathodic transfer coefficient,α_a	2
H_2 Concentration dependence exponent γ_{H2}	0.5
O_2 Concentration dependence exponent γ_{O2}	1.
Backing layer porosity, ε	0.4
Membrane porosity, ε_m	0.28
Membrane Volume fraction in the Catalyst layer , ε_{mc}	0.5
Fixed charge concentration, C_f	1.2 E-3 mol/cm^3
Reference hydrogen concentration $C_{H2,ref}$	40. mol/cm^3
Reference oxygen concentration $C_{O2,ref}$	40. mol/cm^3
Gas channel length, L	7.112 cm
Gas channel width	0.0762 cm
Backing layer width	0.0254 cm
Catalyst layer width	0.00287 cm
Membrane width	0.023 cm

- Most of theses parameters are taken from [7] and [11]

ملخص البحث

تعتبر خلايا الوقود من المصادر الواعدة في مجال إنتاج الطاقة نظرا لما تتميز به من ارتفاع في الكفاءة الحرارية مع انخفاض الانبعاثات الحرارية والصوتية الناجمة عن التفاعلات الداخلية بين الوقود والهواء. كما أنها تتميز بسهولة التشغيل ويمكن توفيرها بقدرات متنوعة تلائم مختلف التطبيقات تسيير السيارات وتوليد الكهرباء.كما يمكن تشغيلها باستخدام أنواع مختلفة من الوقود مما يساهم في سهولة انتشارها كتقنية جديدة في مختلف مواقع الإنتاج.

خلال هذا البحث تم تطوير نموذج رياضى ثنائى الأبعاد، أحادى الطور، مستقر لمحاكاة أداء خلايا الوقود ذات الغشاء البوليمرى Polymer Electrolyte Membrane Fuel Cell.حيث يأخذ هذا النموذج فى اعتباره دراسة معدل التفاعل الكهروكيميائى، ديناميكا الموائع والانتقال متعدد المركبات.

وقد تم استخدام مجموعة واحدة من معادلات الحفظ صالحة للتطبيق خلال المجال غير المتجانس والمكون من قنوات الغازات، الطبقة الإنتشارية Gas Diffusion Layer ،طبقة المحفز والغشاء البوليمرى. وحلها باستخدام برنامج PEMCU والذى تم تطويره خصيصا لحل هذا النموذج الرياضى بناءا على برنامج TEAM الذى تم تطويره عام ١٩٨٤ بجامعة مانشستر الإنجليزية لدراسة نفاث اضطرابى مرتطم.

هذا وقد قام الحل العددى بإلقاء الضوء على التأثيرات المتداخلة والمعقدة بين الكيمياء الكهربية، ميكانيكا الموائع والانتقال متعدد المركبات داخل الخلية.وقد تم استخدام البرنامج العددى فى دراسة تأثير عوامل التشغيل المختلفة على أداء هذا النوع من الخلايا مثل الضغط، درجة الحرارة،نسبة الهيدروجين فى الخليط...الخ. وتمت مقارنة الحل العددى الناتج بالتجربة العملية والحلول العددية المتاحة وأثبتت المقارنة وجود اتفاق جيد بينهم.

نمذجة رياضية ومحاكاة عددية لخلايا الوقود ذات الغشاء البوليمرى

إعداد
مهندس/ **عمار محمد عبد الغنى محمد**

رسالة مقدمة إلى كلية الهندسة، جامعة القاهرة
كجزء من متطلبات الحصول على درجة الماجستير
في هندسة القوى الميكانيكية

يعتمد من لجنة الممتحنين

الأستاذ الدكتور/ **سمير محمد عبد الغنى**	**عضو**
الأستاذ الدكتور/ **محسن محمد مرسى أبو الليل**	**عضو**
الأستاذ الدكتور/ **هاني أحمد صفي الدين خاطر**	**مشرف رئيسى**
الأستاذ الدكتور/ **هنداوي سالم محمد**	**مشرف**

كلية الهندسة ، جامعة القاهرة
الجيزة ، جمهورية مصر العربية
٢٠٠٤

نمذجة رياضية ومحاكاة عددية لخلايا الوقود ذات الغشاء البوليمرى

إعداد

مهندس/ **عمار محمد عبد الغنى محمد**

رسالة مقدمة إلى كلية الهندسة، جامعة القاهرة
كجزء من متطلبات الحصول على درجة الماجستير
في هندسة القوى الميكانيكية

تحت إشـــراف

الأستاذ الدكتور/ **هاني أحمد صفي الدين خاطر**
قسم هندســة القوى الميكانيكية
كليـة الهندســة، جامعــة القاهـرة

الأستاذ الدكتور/ **هنـداوي سالـم محمـد**
قسم هندســة القوى الميكانيكية
كليـة الهندســة، جامعــة القاهـرة

الدكتور/ **عمـرو محمـد علي عبـد الرءوف**
قسم هندســة القوى الميكانيكية
كليـة الهندســة ، جامعــة القاهـرة

كليــة الهندســة ، جامعــة القاهـرة
الجيـزة ، جمهوريــة مصـر العربيــة
٢٠٠٤

نمذجة رياضية ومحاكاة عددية لخلايا الوقود ذات الغشاء البوليمرى

إعداد

مهندس/ **عمار محمد عبد الغنى محمد**

رسالة مقدمة إلى كلية الهندسة، جامعة القاهرة
كجزء من متطلبات الحصول على درجة الماجستير
في هندسة القوى الميكانيكية

كليــة الهندســة ، جامعــة القاهــرة
الجيـزة ، جمهوريـة مصـر العربيــة
٢٠٠٤